

AD _____

Award Number:
W81XWH-04-1-0590

TITLE:
Constrained Adaptive Beamforming for Improved Contrast in Breast Ultrasound

PRINCIPAL INVESTIGATOR:
William F. Walker, Ph.D.

CONTRACTING ORGANIZATION:
University of Virginia
Charlottesville, VA 22908

REPORT DATE:
June 2008

TYPE OF REPORT:
Final Addendum

PREPARED FOR: U.S. Army Medical Research and Materiel Command
Fort Detrick, Maryland 21702-5012

DISTRIBUTION STATEMENT: (Check one)

Approved for public release; distribution unlimited

The views, opinions and/or findings contained in this report are those of the author(s) and should not be construed as an official Department of the Army position, policy or decision unless so designated by other documentation.

REPORT DOCUMENTATION PAGE

Form Approved
OMB No. 074-0188

Public reporting burden for this collection of information is estimated to average 1 hour per response, including the time for reviewing instructions, searching existing data sources, gathering and maintaining the data needed, and completing and reviewing this collection of information. Send comments regarding this burden estimate or any other aspect of this collection of information, including suggestions for reducing this burden to Washington Headquarters Services, Directorate for Information Operations and Reports, 1215 Jefferson Davis Highway, Suite 1204, Arlington, VA 22202-4302, and to the Office of Management and Budget, Paperwork Reduction Project (0704-0188), Washington, DC 20503

1. AGENCY USE ONLY (Leave blank)	2. REPORT DATE June 2008	3. REPORT TYPE AND DATES COVERED Final Addendum, 1 JUN 2004 - 31 MAY 2008
----------------------------------	-----------------------------	--

4. TITLE AND SUBTITLE Constrained Adaptive Beamforming for Improved Contrast in Breast Ultrasound	5. FUNDING NUMBERS W81XWH-04-1-0590
--	--

6. AUTHOR(S) WILLIAM F. WALKER WFW5H@VIRGINIA.EDU

7. PERFORMING ORGANIZATION NAME(S) AND ADDRESS(ES) University of Virginia Charlottesville, VA 22904-4195
--

8. PERFORMING ORGANIZATION REPORT NUMBER
--

9. SPONSORING / MONITORING AGENCY NAME(S) AND ADDRESS(ES) U.S. Army Medical Research and Materiel Command Fort Detrick, Maryland 21702-5012

10. SPONSORING / MONITORING AGENCY REPORT NUMBER
--

11. SUPPLEMENTARY NOTES

12a. DISTRIBUTION / AVAILABILITY STATEMENT Approved for Public Release; Distribution Unlimited

12b. DISTRIBUTION CODE

13. ABSTRACT (Maximum 200 Words) Ultrasonic imaging plays an important role as an adjunct to mammography, with an emerging role in breast cancer screening. Ultrasound's real-time nature, lack of ionizing radiation, and relative comfort for the patient make it an attractive imaging choice. Unfortunately, ultrasound image quality is often limited. We hypothesize that bright scatterers seriously degrade ultrasound images by introducing image clutter. In the breast bright off-axis echoes may originate from Cooper's ligaments, structured glandular tissue, calcification, fat-soft tissue interfaces, or other structures. We initially proposed using a variant of the Frost Adaptive Beamformer to reduce clutter, but discovered that this technique is non-optimal for our application. Extensive literature review led us to modify the Spatial Processing Optimized and Constrained algorithm (SPOC) to yield the Time-Domain Optimized Near-field Estimator (TONE). In simulations and phantom experiments this technique yields dramatic improvements in resolution and contrast. We have also developed alternate methods of image formation (LCLS and QCLS) that are computationally simpler and, while less impressive than TONE, also yield dramatic image improvements.

14. SUBJECT TERMS Imaging, Ultrasound, Diagnosis, Non-invasive

15. NUMBER OF PAGES 57
16. PRICE CODE

17. SECURITY CLASSIFICATION OF REPORT Unclassified

18. SECURITY CLASSIFICATION OF THIS PAGE Unclassified
--

19. SECURITY CLASSIFICATION OF ABSTRACT Unclassified

20. LIMITATION OF ABSTRACT Unlimited

Table of Contents

Introduction.....	5
Body.....	7
Key Research Accomplishments.....	22
Reportable Outcomes.....	23
Conclusions.....	24
References.....	24
Appendices.....	26

Introduction:

Ultrasonic imaging plays an important role as an adjunct to mammography [1, 2]. Ultrasound's real-time nature, lack of ionizing radiation, and relative comfort for the patient make it an attractive choice for applications which include the differentiation of fluid filled cysts and solid masses, differentiation of benign and malignant lesions, and guidance of needle and core biopsy procedures. Recent studies have even shown the potential of ultrasound as a screening tool, especially for pre-menopausal women whose radio-dense breast tissue seriously limits x-ray mammography [3]. In both differential diagnosis and screening applications however, ultrasound image quality is limited, with high levels of background clutter representing a significant problem in many patients.

While the cause of high background clutter and poor breast image quality has not been determined with certainty, it is widely held that acoustic velocity inhomogeneities in breast tissue cause defocusing of the acoustic beam. This distortion manifests itself through mainlobe broadening and increasing sidelobe levels. Numerous researchers, including the Principal Investigator, have suggested that this problem, known as phase aberration, might be corrected through the application of compensating time delays [4-6], a combination of delay and amplitude corrections [7], or other more complex techniques [8-10]. While proposed phase aberration correction methods have been shown to have great potential in *ex vivo* or other non real-time environments, there has been limited evidence of significant clinical image improvement. The development of a real-time phase aberration correction system at the GE Global Research Center has shown that real-time phase correction is possible, however *in vivo* results using 1.5-D arrays show contrast improvements of only about 3 dB in the abdomen [11, 12]. This unimpressive outcome may result from imperfect algorithm optimization, or perhaps a lower level of *in vivo* phase aberration than previously suspected. This latter hypothesis is supported by phase aberration measurements performed at Duke University which indicate *in vivo* phase aberrations of only ~25ns RMS (Root Mean Squared) with a 3.5 mm FWHM (Full Width at Half Maximum) [13]. The limited improvements of real-time phase correction, coupled with low measured aberrations, suggest that phase aberration may not represent the major source of breast image degradation.

If phase aberration is not the primary factor limiting breast image quality, then what is? We hypothesize that localized bright scatterers seriously degrade ultrasound images by introducing broad image clutter. Figure 1 shows single channel Radio Frequency (RF) echo data obtained from calcifications in the thyroid of a human subject at Duke University. A focused transmit beam was used and RF data was acquired from each element in a 1.5-D array consisting of approximately 1000 elements. Figure 1 shows data from one row of this array after application of geometrically determined focal delays. At least three clear waveforms are visible in this data set, with each probably resulting from a single calcification. Although summation across channels to form an RF image line would amplify the echo coming from directly in front of the array, it would not entirely eliminate the two other visible targets. These non-focal targets would appear in this image line as clutter, reducing image contrast. In addition to the three dominant calcification waveforms, the data set also includes echoes from background speckle. These background echoes also include discernable off-axis scatterers that undoubtedly generate further clutter in the image. Note that the thyroid data presented in figure 1 is similar in appearance to breast data obtained at Duke. In the breast bright off-axis echoes may originate from Cooper's ligaments, highly structured glandular tissue, calcification, fat-soft tissue interfaces, or other tissue structures.

The presence of bright off-axis scatterers and the image degradation that they cause is not surprising. It is well known that the acoustic reflectivity of targets within the body covers many orders of magnitude. It is precisely for this reason that manufacturers employ aggressive apodization to reduce sidelobe levels in diagnostic ultrasound. It has also been argued that harmonic imaging is effective at improving image quality because it further reduces sidelobe levels and therefore reduces the spatial spread of bright targets. The detrimental impact of bright scatterers on ultrasound image quality is recognized in experimental data, physical intuition, and years of experience in ultrasound system design.

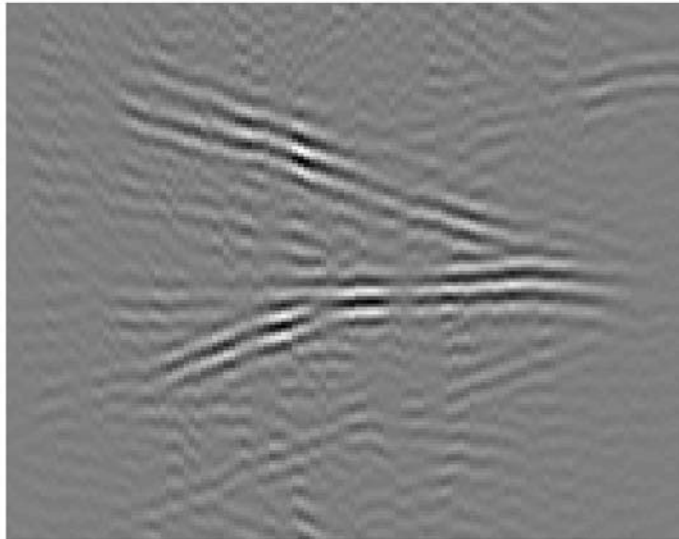


Figure 1: Single channel data obtained *in vivo* from a human thyroid. At least three bright scatterers (likely microcalcifications) are visible. While one target lies near the focus, the other two are off-axis and will contribute clutter to this image line. Off-axis targets are also visible within the speckle generating background echoes. (Data courtesy Gregg Trahey, Duke University.)

The impact of a few bright targets in an otherwise dim image has been well studied in both RADAR and SONAR. In SONAR the detection of an intentionally stealthy submarine among many noisy ships requires separating out a signal that is orders of magnitude below the signals from other nearby targets. A broad variety of adaptive beamforming algorithms have been developed for this scenario. It is the goal of this research project to evaluate the potential applicability of these methods in medical ultrasound.

Body:

Summary of Accomplishments:

Over the course of this project our research broadened significantly beyond the original proposal. Our original goal of evaluating and improving upon the Constrained Adaptive Beamformer (CAB) was superseded by the development of an entirely new family of algorithms which we have come to name TONE for Time Domain Optimized Near-field Estimator [14]. TONE has been experimentally to achieve spatial resolution and 10 times better than conventional imaging methods. Our research into TONE and its potential led to a number of other associated developments. The major accomplishments were:

- Development and application of a new cyst resolution metric for assessing ultrasound image quality
- Development of a new class of FIR beamformers
- Improvement and evaluation of adaptive imaging algorithms based loosely on SPOC
 - Invention and testing of the basic TONE algorithm for image reconstruction
 - Invention of diffuse TONE (dTONE) to enable more robust imaging of real-world targets
 - Invention of the quick TONE (qTONE) algorithm for dramatically faster image reconstruction
 - Application of TONE, dTONE, and qTONE to *in vitro* and *in vivo* imaging
- Development of a new spline based method of simulating ultrasound propagation

In aggregate these accomplishments place a new fundamental foundation under ultrasound image formation. We now realize that so called “physical limits” on resolution are really an artifact of our image formation methods and that by employing new methods we can dramatically improve image quality. We have also developed an array of tools to simulate ultrasound beamforming and to rigorously compare the performance of different beamformers.

The FIR beamforming approach developed under this grant is patent pending and has been licensed from the University of Virginia to Pocket Sonics, a company co-founded by this grant’s Principal Investigator. Two patents are currently pending to protect the TONE and qTONE algorithms. The Principal Investigator is in the process of forming a company to license and commercialize these technologies. Together these commercialization efforts indicate a strong opportunity to apply these research developments to improve clinical treatment and diagnosis of breast cancer.

A Metric for Assessing Beamformer Performance:

The literature in ultrasound imaging, as well as SONAR and RADAR, is littered with novel beam forming strategies, new apodization functions, and “optimal” imaging strategies. Unfortunately traditional measures of beamformer quality, such as Full Width at Half Maximum (FWHM) of the beamplot are not well suited to quantify the performance of medical ultrasound imaging systems, where true point targets are rare, but diffuse targets are common. This disparity has meant that many algorithms that appear promising for point target imaging are not useful in clinical settings. Some time ago we realized that a new measure of beamformer performance was needed; one that was more in tune with clinical problems.

We have derived a novel metric for quantifying ultrasound image quality. Unlike traditional measures, such as the Rayleigh resolution, which quantify point target resolution, our metric quantifies the contrast of an anechoic cyst as a function of cyst radius. Cystic contrast is a much more relevant parameter for medical ultrasound where point targets are rare and of little clinical importance. Our first paper describing this new metric was published in April 2007 [15].

This original metric was somewhat limited in that it only considered the impact of electronic noise through a Signal to Noise Ratio (SNR) on the summed echo signal. This made it awkward to compare the impact of apodization on SNR directly, as it did not explicitly consider the SNR on individual beamformer channels. We developed a new cystic resolution metric that considers individual channel SNR, and therefore allows direct

comparison across various apodization functions. This metric allows the designer to identify “optimal” apodizations that incorporate both realistic propagation physics and the impact of electronic noise. In our early work with this metric we have identified a tradeoff between idealized image contrast and electronic noise; a tradeoff that we have not seen considered explicitly elsewhere. A paper describing this metric was published in 2009 [16].

Conventional Beamformer Optimization:

While the TONE and dTONE algorithms (described in detail below) offer tremendous improvements in resolution and contrast, their high computational cost presents a challenge to short-term, real-time implementation. Further, while we know that these algorithms significantly outperform existing beamformers, we do not know that such conventional delay and sum beamformers are “optimal” in the sense of achieving the best possible contrast or resolution. Thus, to offer a better chance of short-term technology gains and to provide a true benchmark for comparison, we have developed two novel techniques for optimizing conventional delay and sum beamformer performance. These techniques, termed Linear Constrained Least Squares (LCLS) and Quadratically Constrained Least Squares (QCLS) optimization design optimal beamformer weights using slightly different mathematical criterion. LCLS minimizes the point spread function energy outside a given cyst radius while maintaining a constant gain at the center of the cyst. This technique yields a closed form solution that makes best use of the element responses, regardless of system non-idealities including limited element angular response, near field variations, and finite bandwidth. The second technique, QCLS, also minimizes the point spread function energy outside a given cyst radius, but constrains the energy within the cyst radius. This technique effectively optimizes the cystic contrast metric and therefore should optimize image quality. The theoretical underpinnings and simulation validation of these techniques are described in two papers published in IEEE Transactions on Ultrasonics, Ferroelectrics, and Frequency Control [17,18].

The FIR Beamformer:

The LCLS and QCLS design techniques are guaranteed to yield optimal apodization profiles for a given imaging system, however with only one parameter to adjust on each beamformer channel, we found that the optimal performance was not always much better than conventional apodization. As we reflected upon this, we wondered if it was possible to define a beamformer architecture wherein we could adjust multiple parameters on each channel and thereby achieve greater gains in performance. The beamformer architecture we envisioned is shown below in figure 2. The upper panel depicts a conventional delay and sum beamformer where the parameters W , X , and Y are the designed apodizations. The lower panel depicts the new FIR beamformer architecture in which a 3 tap FIR filter is placed on each beamformer channel, after the delay stage. (Note that the abbreviation FIR stands for Finite Impulse Response.) In this beamformer the parameters A , B , C , ... N , and O are designed in the numerical optimization.

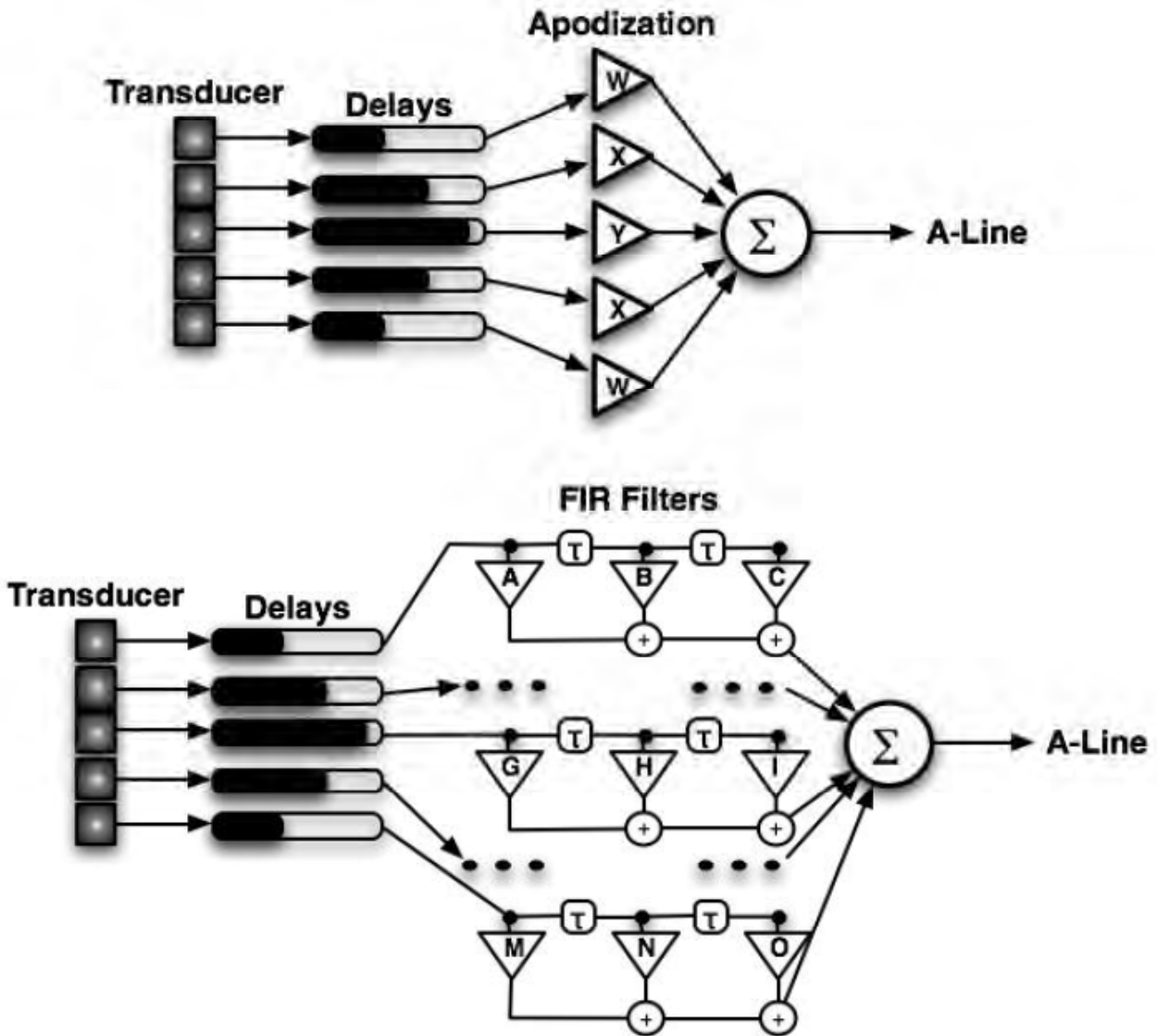


Figure 2: Conventional and FIR beamformer architectures. The upper panel depicts a conventional delay and sum beamformer with a single adjustable apodization value per channel. The lower panel depicts the novel FIR beamformer architecture in which multiple weights are applied to each channel. In this particular realization three filter taps are used on each channel, although there is no theoretical limit to the number of taps that can be applied.

This greater degree of flexibility afforded the FIR beamformer yields dramatic, and robust increases in performance. In our current design methodology we simply apply the QCLS design method, but design for multiple, temporally delayed apodization profiles to obtain channel dependent FIR filter coefficients. Because this method forms FIR filters on each channel it is able to effectively perform frequency dependent beamforming to achieve optimal broadband results. Figure 3 shows significant experimental improvements in lateral resolution and contrast achievable with the FIR beamformer. Note that the FIR beamformer achieves both a narrower mainlobe and a lower sidelobe level than conventional beamforming. These benefits have a significant impact on cystic contrast, improving cystic contrast by over 10 dB.

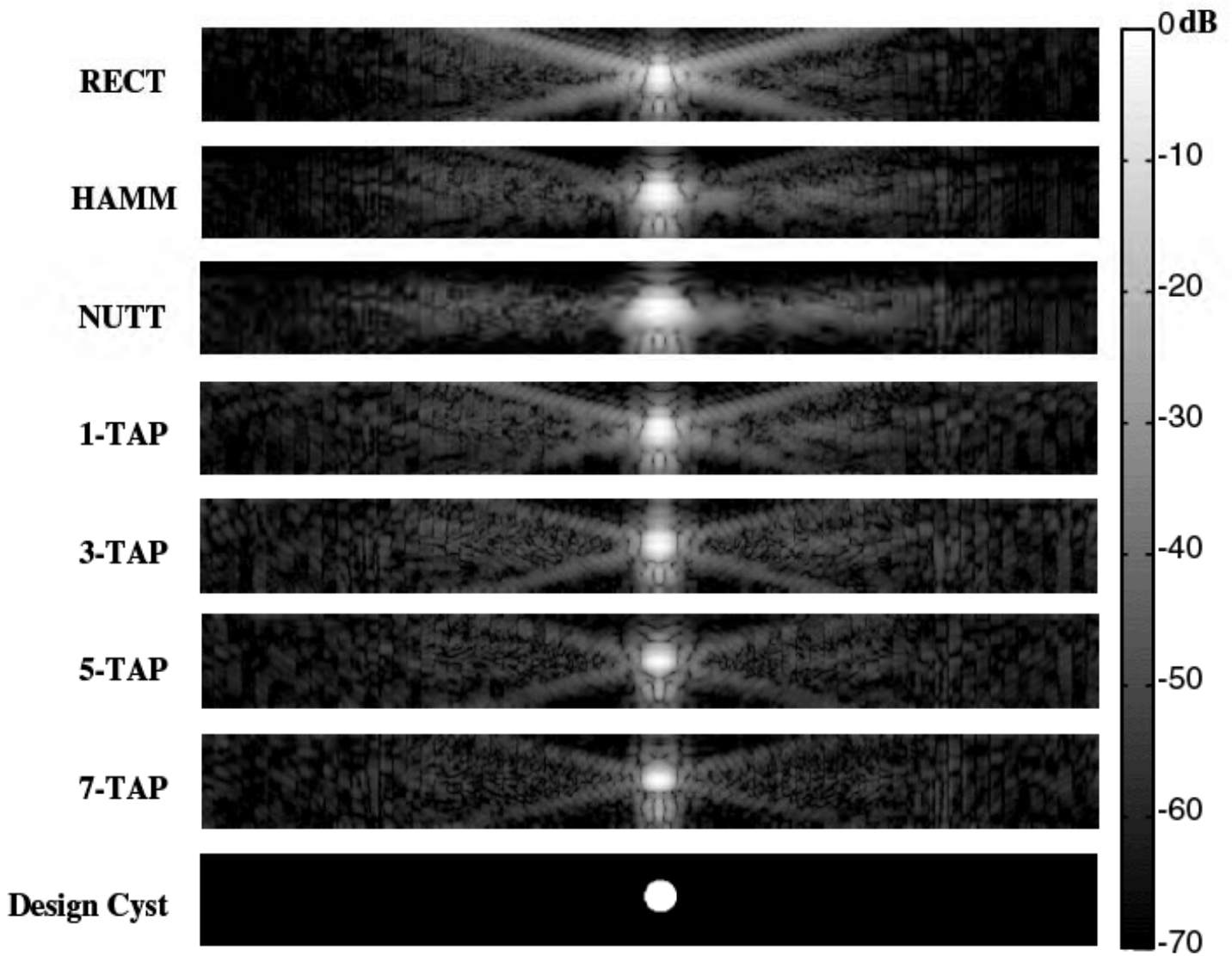


Figure 3: Experimental 2D PSFs with different receive apodization functions applied. Each image is 0.2 cm axially by 1.95 cm laterally. All images were envelope detected and log compressed to 70 dB. The conventional windows' PSFs suffer from high sidelobes and wide mainlobes. The multi-tap FIR-QCLS apodization functions progressively reduce the total sidelobe energy while maintaining a tight mainlobe in the spatial PSFs. The design cyst is shown for reference.

We further assessed the performance improvements of the FIR beamformer by convolving the experimentally obtained point spread functions with simulated cysts within a speckle generating background. The simulated images, shown below in figure 4, show an appreciable improvement in cystic contrast with FIR beamforming.

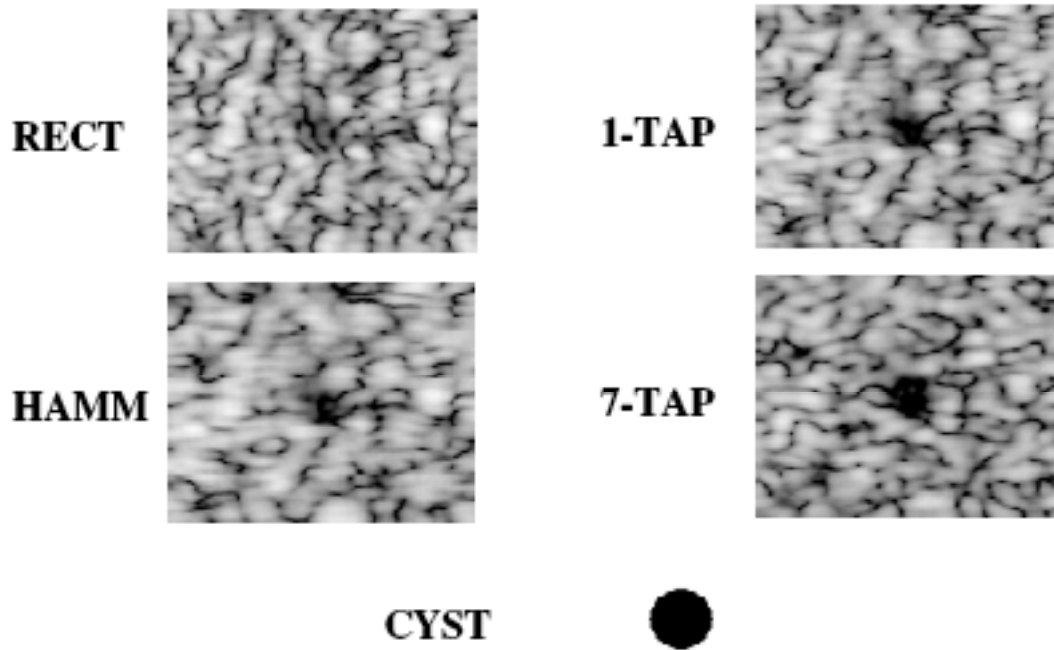


Figure 4: Simulated B-mode images of a 1.0 mm diameter cyst embedded in speckle using the experimental PSFs. All images are log compressed to 30 dB and show a 5 mm by 5 mm area surrounding the anechoic cyst. The 1.0 mm diameter cyst is shown for reference.

Time-Domain Optimized Near-Field Estimator (TONE):

For nearly four decades, adaptive beamforming (ABF) algorithms have been applied in RADAR and SONAR signal processing. These algorithms reduce the contribution of undesired off-axis signals while maintaining a desired response along a specific look direction. Typically, higher resolution and contrast is attainable using adaptive beamforming at the price of an increased computational load. We have developed a novel ABF designed for medical ultrasound, named the Time-domain Optimized Near-Filed Estimator, or TONE. The novel ABF was developed from Spatial Processing: Optimized and Constrained (SPOC) technique originally developed by Van Trees *et al.* for applications in passive SONAR [20]. TONE is well suited to medical ultrasound since it requires neither a far-field/narrow-band assumption nor second order statistics of the signals. As seen below, TONE shows a significant improvement in resolution and contrast when compared to conventional, data independent beamforming.

TONE Progress:

The region of tissue to be imaged region (the region of interest or ROI), is subdivided into a collection of hypothetical targets at arbitrary positions, as shown in figure 5. Finer target placement yields finer final image resolution but entails higher computational costs. For each hypothetical target in the ROI, we model the signal received by the array for that specific point (i.e., the spatial responses). These spatial responses can be determined using a theoretical model, computational model, or can be extracted from experimental data. For every hypothetical target, the spatial impulse response is a matrix of dimensions $T \times N$, where T is the number of samples in the time dimension and N is the number of elements in the array. After the spatial impulse responses for all the hypothetical targets have been calculated, these responses are reshaped to form an array manifold matrix \underline{V} of dimensions $NT \times LP$, where L and P are the numbers of hypothetical sources in the range and lateral dimensions, respectively. The observation model then becomes:

$$\underline{x} = \underline{V} \underline{f} \quad (1)$$

where $\underline{x} = [\underline{x}_1 \ \underline{x}_2 \ \dots \ \underline{x}_N]^T$ is the data received by the N -element array and \underline{f} is the $LP \times 1$ target amplitude vector, whose elements are the amplitudes of the hypothetical targets located in the ROI. \underline{x} is a $NT \times 1$ vector that is obtained by concatenating the $T \times 1$ channel data \underline{x}_i . Given \underline{x} and \underline{V} , TONE matches the received data \underline{x} to the signal model to solve for the position and intensity of the real sources (i.e., the \underline{f} vector). If there is no real source at a particular location within the ROI, then the element of \underline{f} that corresponds to that location should be zero. Mathematically, this is accomplished by solving the following maximum a posteriori (MAP) optimization problem:

$$\begin{aligned} \text{Cost function: } & \sum_{i=1}^{LP} \ln |f_i|^2 \\ \text{subject to: } & \underline{x} = \underline{V} \underline{f} \end{aligned} \quad (2)$$

where f_i are elements of \underline{f} . A solution for the MAP optimization problem is found using the following iterative procedure described by K. W. Lo.

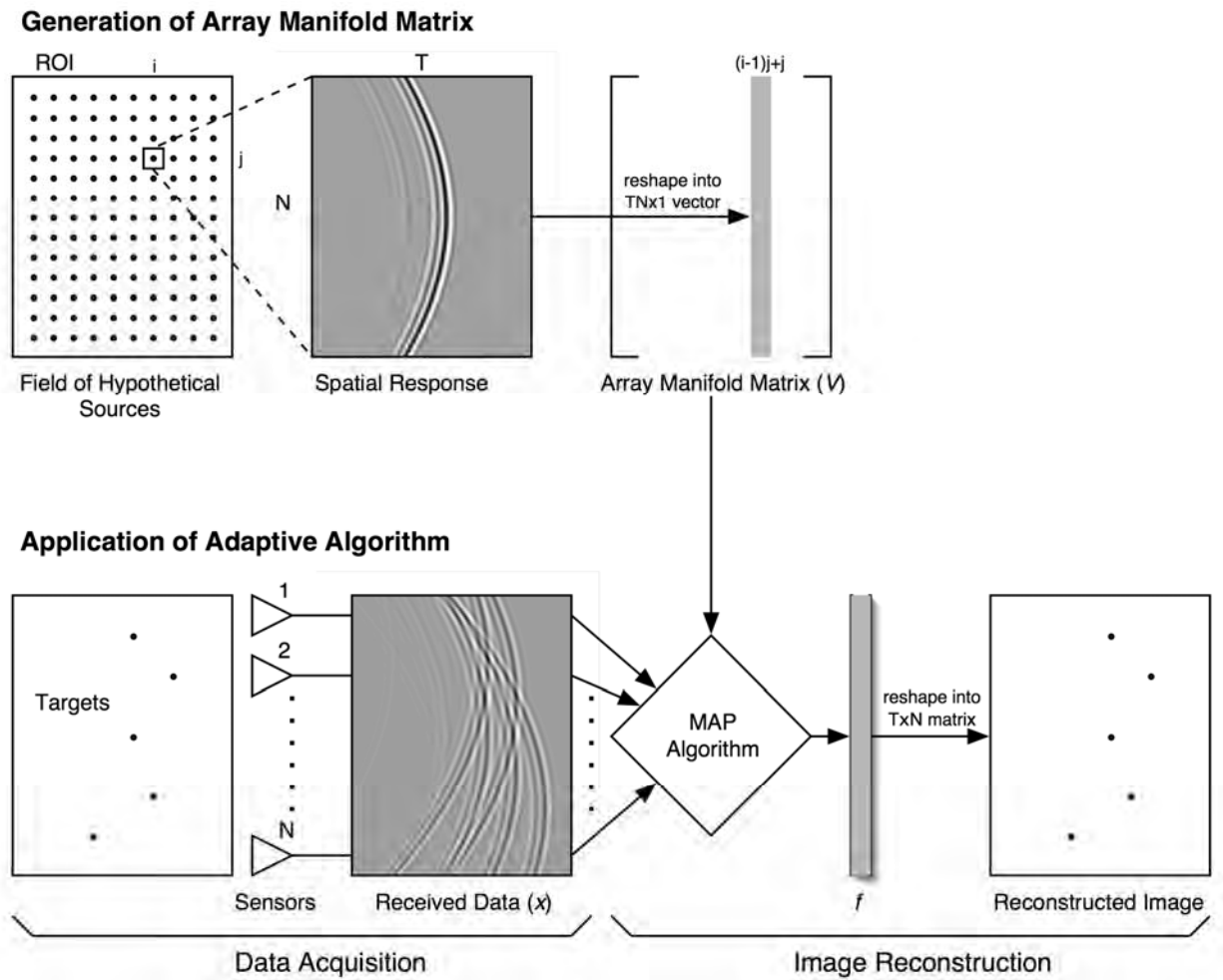


Figure 5. Schematic diagram of TONE.

A series of computer simulations were performed in Matlab to test the potential of TONE. These simulations and their results are described in detail below.

Single Point Target Simulations

A point target was placed directly in front of the transducer at a depth h of 20.1mm. We simulated a 33 element linear array operating at 5 MHz with element spacing of 150 μ m. Signals were sampled at 40 MHz. Plane wave transmission was used for conventional beam forming and SPOC. Conventional beamforming was applied on the received RF data using Hann apodization and dynamic receive focusing. For SPOC, we discretized the image region as a set of hypothetical targets separated 20 μ m in range and 100 μ m in azimuth.

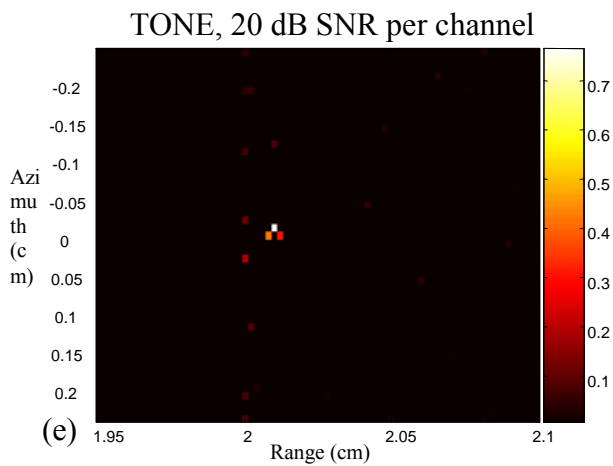
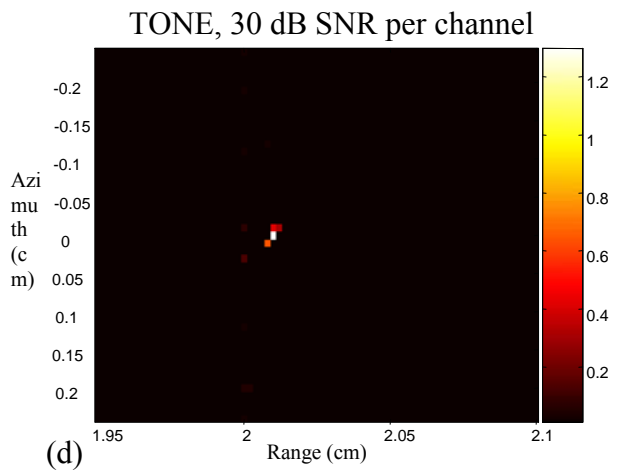
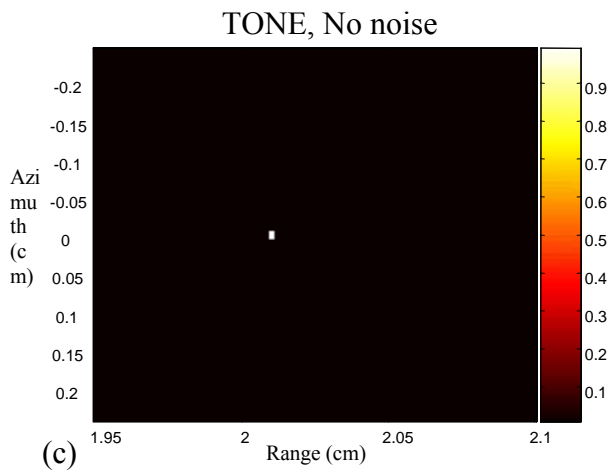
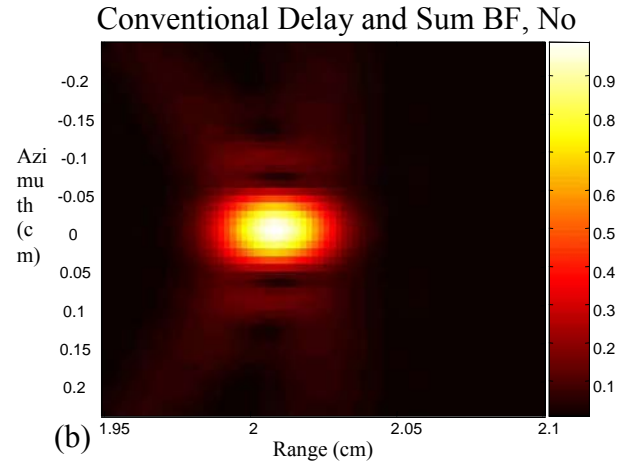
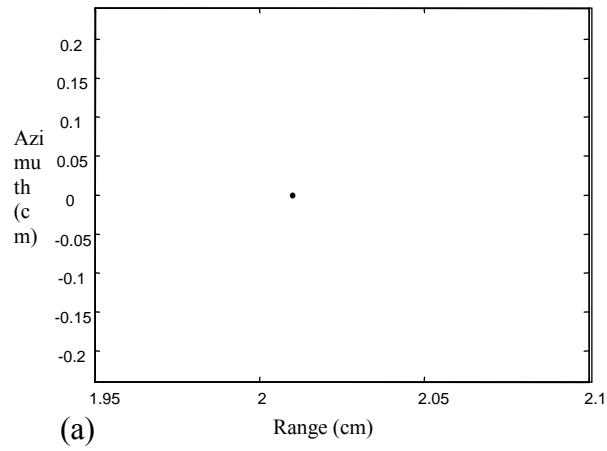


Figure 6. Point target simulations. The point target is depicted in (a); (b) shows conventional delay-and-sum beamforming, whereas images (c) to (e) show SPOC with different levels of electronic noise.

Multiple Point Target Simulations:

A series of point targets were distributed within a 4x5mm region in range and azimuth, respectively. In this case, we simulated a 33 element linear array operating at 5 MHz with element spacing of 150μm. The final

sampling frequency was set at 40 MHz. A plane wave was used on transmit for both conventional beamforming and TONE. Conventional beamforming was applied on the received RF data using Hann apodization and dynamic receive focusing.

For TONE, we discretized the image region in a set of hypothetical target locations separated 20 cm in range and 120 cm in azimuth. The positions of the points were chosen so that some, but not all coincide with the positions of the hypothetical targets. Results are encouraging in that they show TONE is robust to differences between true target location and model target location.

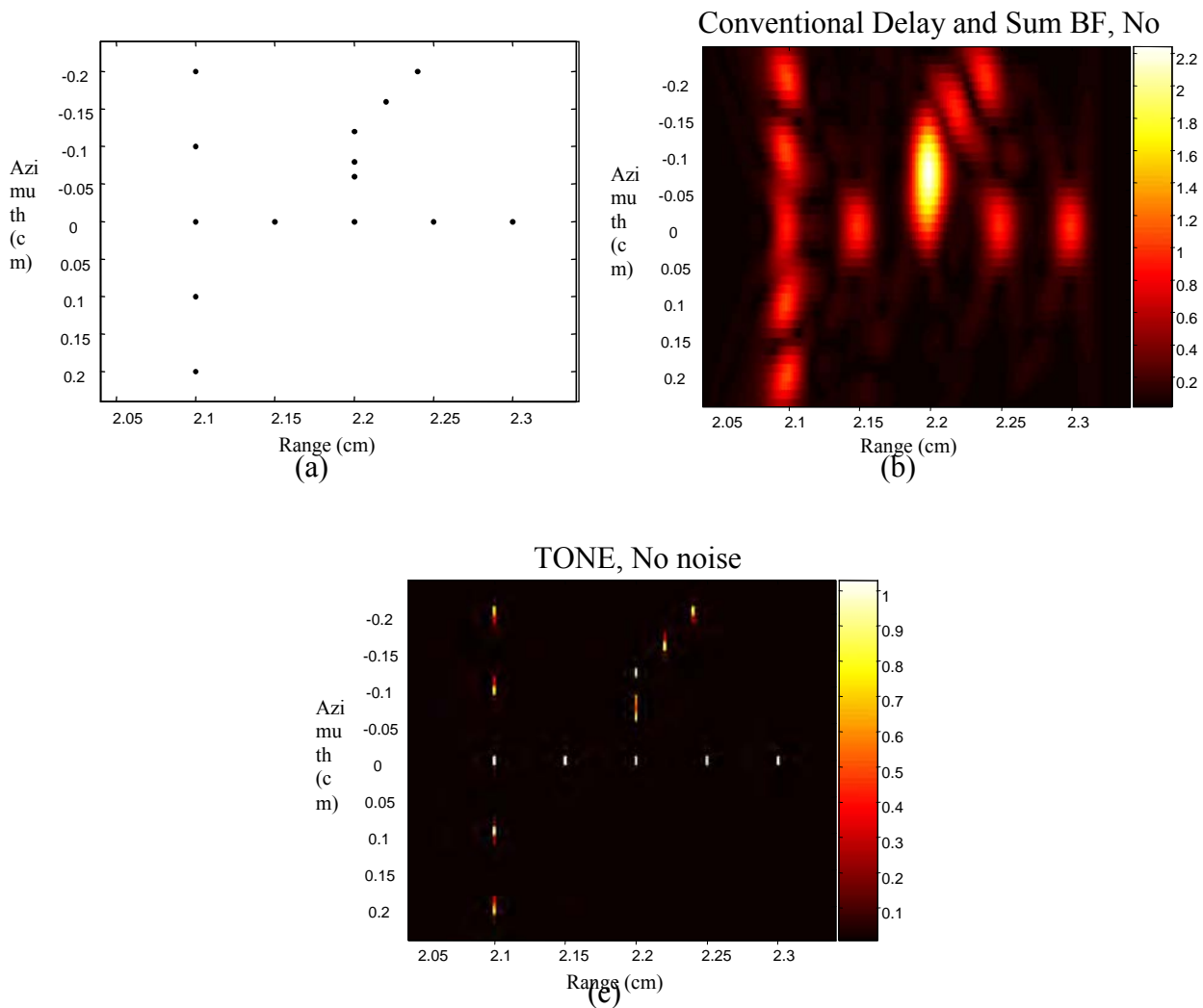


Figure 7. Results obtained simulating a series of wire targets. The wires are depicted in (a); (b) shows conventional delay-and-sum beamforming, whereas (c) show TONE.

Anechoic Cyst Simulation:

A 1mm radius anechoic cyst was placed in front of the array and surrounded by ultrasonic scatterers randomly distributed within the image region. Scatterer amplitudes followed a Gaussian distribution with zero mean and standard deviation of one. Simulation methods are the same of those described in the previous section, except that the hypothetical source sampling was reduced to 100 cm in azimuth. Again, the positions of the scatterers do not necessarily coincide with the position of the hypothetical sources. Results indicate that SPOC is robust in the presence of large numbers of targets placed at intervals closer than the conventional resolution.

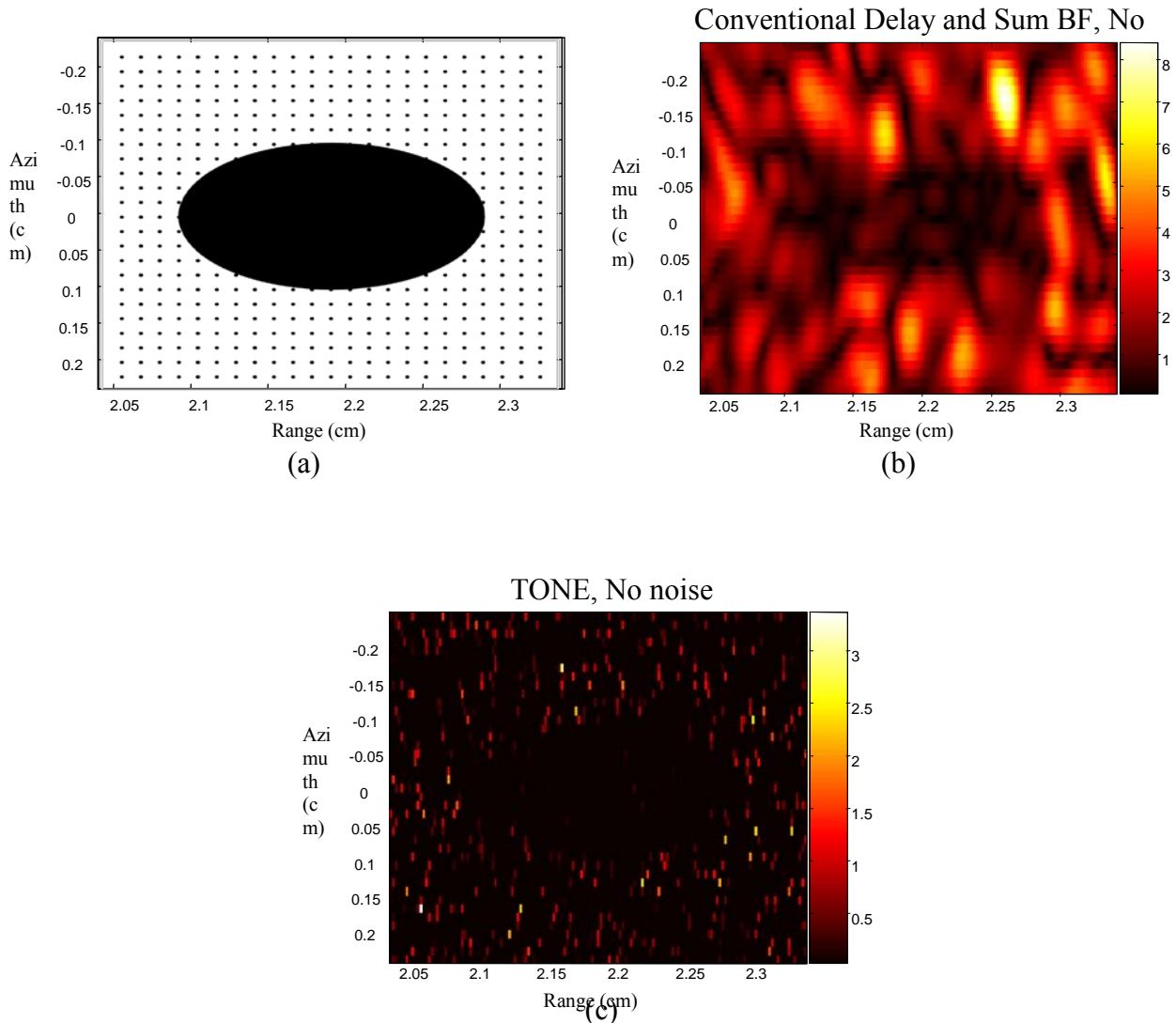


Figure 8. Results obtained simulating an anechoic cyst surrounded by scatterers. The cysts is depicted in (a); (b) shows conventional delay-and-sum beamforming, whereas (c) show TONE.

Experimental results:

We also performed a series of experiments using a commercially available Philips SONOS 5500 i imaging scanner and a series of 5 wires suspended in a water tank. The wires are 20 μm in diameter and spaced roughly 2mm apart. The top panel of figure 5 shows the image generated by the Philips scanner, whereas the bottom panel shows the TONE reconstructed image. In the case of TONE we discretized the image region in a series of hypothetical targets separated by roughly 20 μm in both range and azimuth. Results indicate that TONE can perform robustly with real experimental data. Further work is ongoing to test TONE in excised tissues.

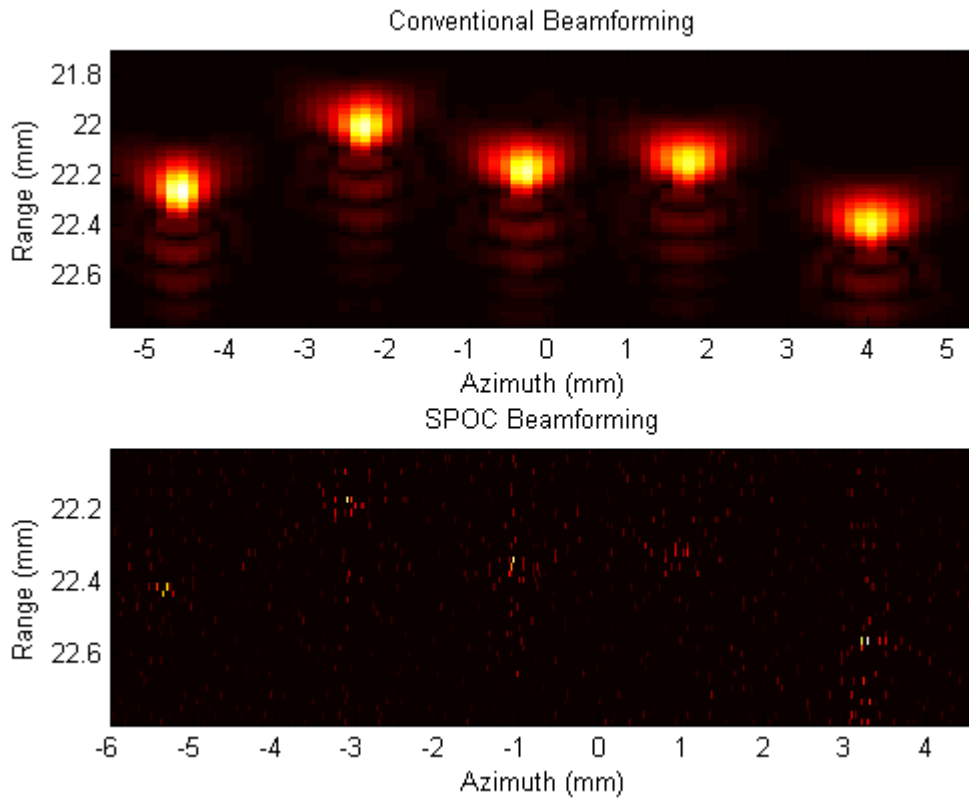


Figure 9. Comparison between conventional beamforming (top) and TONE [formerly called SPOC] (bottom) on a set of 5 wires suspended within a water tank. The wires are 20 μm in diameter.

Diffuse Target TONE (dTONE):

One of the limitations of TONE is that it assumes that the imaged targets lie at discrete locations within the body, an assumption that is clearly not true in practice. While the impact of this assumption can be mitigated to some extent by more finely sampling the hypothetical target grid, this approach is extremely costly computationally. Further, in our experience it is not clear that the costs incurred result in a significantly better image. Because of the coherent nature of echo summation, a true target lying between two hypothetical target locations might be best modeled by TONE using a large cloud of scatterers spread over a large region of the reconstructed image. This is both unsightly and not useful. To deal with both of these issues we have developed a new variant of TONE called diffuse target TONE or dTONE.

dTONE reconstructs the image in exactly the same manner as TONE, but by using a slightly array manifold matrix V it is able to robustly account for targets that do not lie precisely on the reconstruction grid. dTONE alters the array manifold matrix by assuming that the signal from one hypothetical target really originates from a diffuse, amplitude weighted group of targets centered about the hypothetical target location. This approach is more computationally costly in the formulation of the problem, i.e. computation of the array manifold and later eigenvalue decompositions, but has absolutely no impact on the computational cost of the reconstruction. Since we anticipate that the array manifold formation and eigenvalue decompositions will be performed offline, this algorithm represents an elegant way to improve performance. When we reconstruct a dTONE image we represent the targets from each hypothetical location using a bi-cubic spline. This approach yields a smoother and more pleasing image. An experimental dTONE image is compared with a TONE image below in figure 10. The dTONE image has less clutter and is visibly smoother.

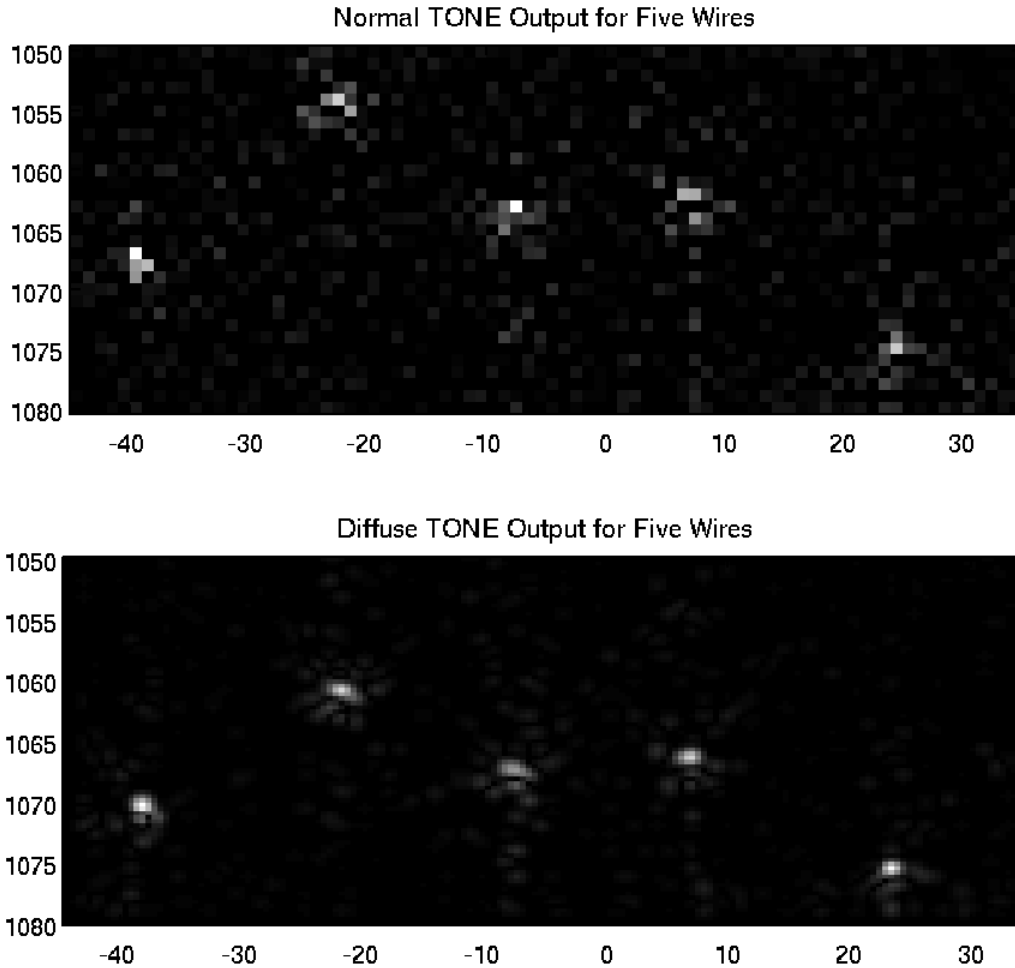


Figure 10. Comparison between experimentally formed TONE and dtONE images.

Simulation Tool Development:

The performance of TONE depends greatly upon the quality of the system model it applies. In our initial simulations we modeled the system using analytical methods, or using the well known FIELD program written by Jørgen Jensen. Unfortunately FIELD is quite slow when computing full 3D spatial impulse responses. Further, because FIELD works entirely on sampled data sets it is prone to artifacts from undersampling. We have implemented the Tupholme-Stepanishen method (the core approach used in FIELD) in a new piece of code we call DELFI. The DELFI code uses cubic spline representations of the transmitted pulse, and the transmit and receive spatial impulse responses. This approach avoids the potential sampling difficulties of FIELD. It is also significantly faster at computing space-space-space responses at an instant in time. These sort of responses are critical in much of our research and the 25 fold increase in speed for DELFI is of great significance. Our paper describing the DELFI code was published this May [19]. Some results from this paper are shown below in figure 11. Note that for space-space responses DELFI is significantly faster to achieve a given accuracy level. For space-time responses DELFI is somewhat slower, but can achieve high accuracy at significantly lower sampling rates. We placed the final version of our DELFI code on the Mathworks web site just after our paper was accepted for publication. This code has been downloaded over 200 times since then.

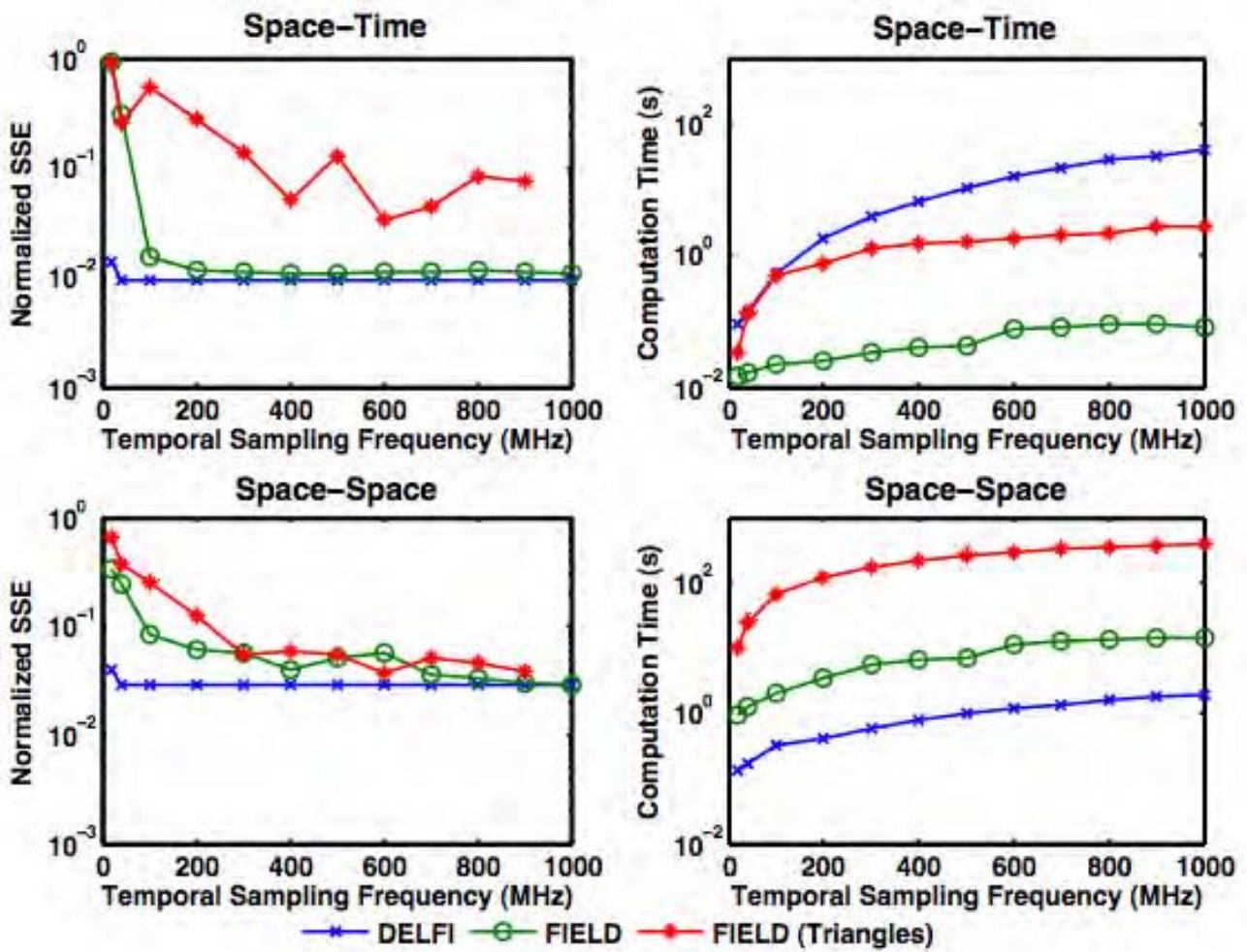
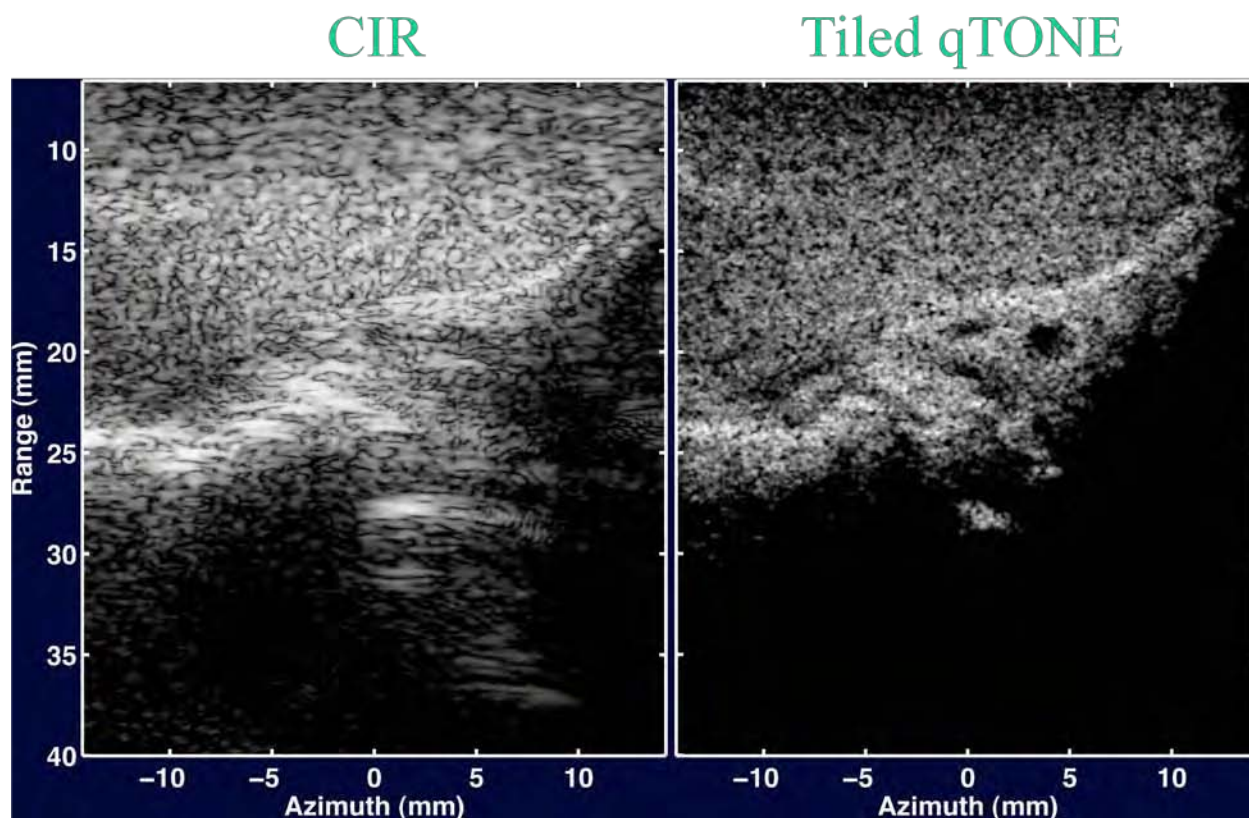


Figure 11: Simulation results comparing the speed and accuracy of DELFI and FIELD (both rectangular and triangular computational elements) for space-space and space-time responses. Note the high accuracy achieved for DELFI at even low sampling rates.

Quick-TONE (qTONE):

In order to further the computational cost of dTONE such that it can be applied to in vivo imaging, a change in the core algorithm is required, leading to the development of qTONE. qTONE shifts the computational cost from being based on the number of hypothetical scatterers to being based on the number of input samples, which allows for significant reductions in reconstruction time with little effect on image quality (please see Appendix 1 for details).

In the final stage of this project we applied the qTONE image reconstruction algorithm to in vivo imaging. The attached images were formed from data obtained from the testicle of a healthy volunteer. As the images show clearly (Fig. 12), qTONE images yield better resolution and contrast than traditional beamforming. Note the numerous ducts which are visible in the qTONE images but are completely absent in the conventionally beamformed images. These images strongly support the potential clinical value of qTONE imaging (please see Appendix 2 for details).



CIR

Tiled qTONE

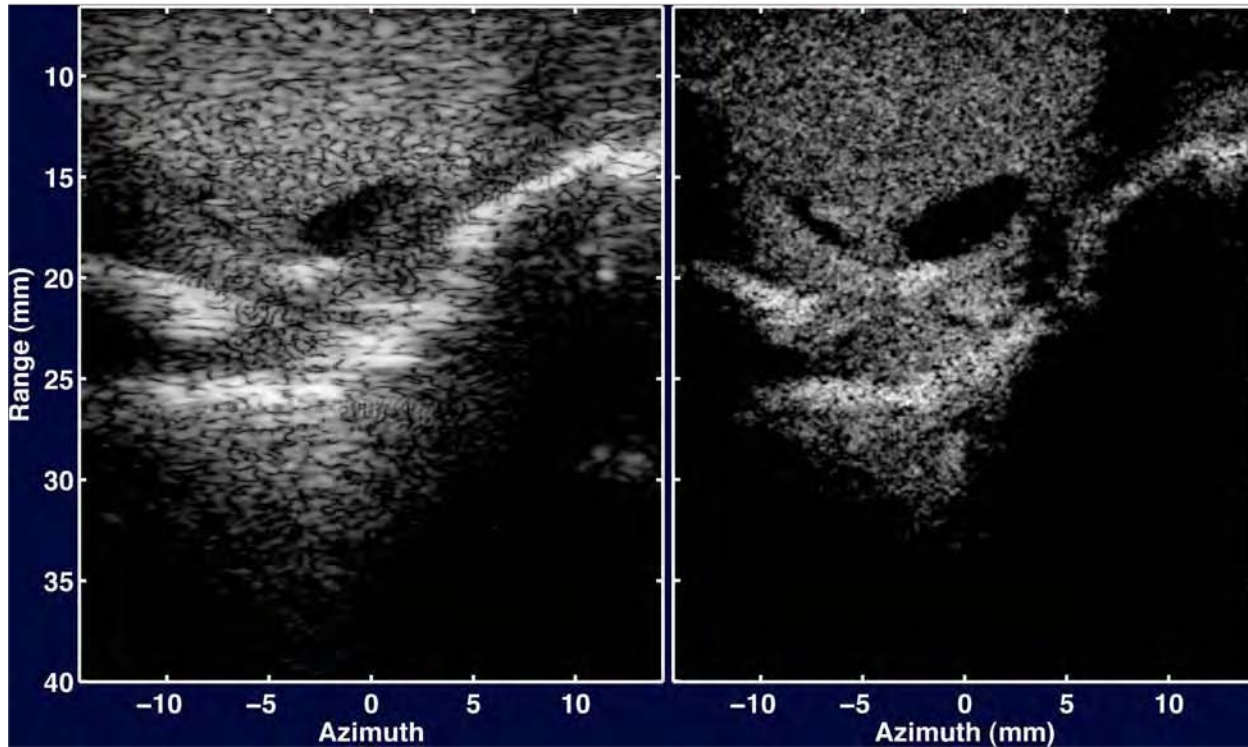


Figure 12. *In vivo* CIR and tiled qTONE images of a human testicle. All images log compressed to 50 dB.

Experimental Platform Development:

During the life of this grant we shifted our experimental work almost entirely to the Ultrasonix Sonix RP. The Sonix RP is a highly programmable research platform built around a clinical ultrasound imaging system. We acquired this system in June 2006 and have since implemented a broad range of tools:

- * Python scripting interface for Ultrasonix, to allow interactive control of all transmit/receive sequences without recompilation, for rapid experiment turnaround.
- * Synthetic receive control - ability to receive single element RF data on successive transmits.
- * Synthetic transmit control - ability to transmit on single elements.
- * Automated full synthetic transmit/receive, this lets us capture full synthetic data sets from a 128-element transducer in 30 seconds.
- * Automated transducer characterization in conjunction with hydrophone.
- * Matlab interface for execution and analysis of simple sequences in a single script.
- * Automated averaging of repeatedly captured data to improve SNR.

While we have made tremendous progress in developing tools for system control and data acquisition, our experimental progress is hampered by the poor quality of the transducer arrays currently sold for the Sonix RP. These transducers exhibit poorer element angular response, poorer element spacing, and poorer bandwidth than state of the art transducers. To circumvent this limitation we are integrating a Philips linear array probe with the Sonix RP. This array is at the state of the art for small parts imaging and when integrated, will be recognized by the Sonix RP as native and thus available for real-time imaging and programmed data acquisition.

Another experimental system, not described in the original proposal, is a fully custom system developed in collaboration with two other investigators at the University of Virginia (John A. Hossack and Travis N. Blalock.) A second generation of this system is being assembled. This second generation system will utilize a 3600 element 2D array and will operate at a 5.0 MHz center frequency. Data from all channels will be acquired in parallel in real-time, however only four real samples will be acquired by each channel. Although the data acquisition of this system is certainly limited in some ways, we believe that this system will provide an excellent testbed for TONE.

Corporate Interactions:

Our work on TONE has great potential, but presents great challenges. We have been assisted in these efforts through a number of valuable corporate interactions.

Our experimental work was originally aided through technical support and equipment donations from Philips Medical Systems. Our transition to the Sonix RP system has of course been supported by UltraSonix.

TONE is extremely challenging to implement computationally and we have worked closely with Interactive Supercomputing to test the algorithm. They have provided technical support to enable the transition of our algorithms to their Star-P MATLAB parallelization software. Interactive Supercomputing has also provided us with free CPU cycles on their high-end cluster.

Key Research Accomplishments:

- Developed and published a new metric to quantify ultrasound beamformer performance.
- Developed and published a second new metric that accurately combines the effects of cystic contrast resulting from the system point spread function and noise on individual beamformer channels.
- Developed and published two new methods for optimizing beamformer apodization functions (LCLS and QCLS design methods.)
- Developed a new ultrasound beamformer architecture (FIR beamformer) that achieves dramatic improvements in image contrast and resolution.
- Developed, tested, and published a new adaptive beamformer, the TONE algorithm.
- Developed, tested, and published a variant of TONE, dTONE which yields smoother images with higher contrast and fewer artifacts.
- Developed and tested another variant of TONE, qTONE which is significantly faster and yields improved image quality.
- Developed and published a new approach to ultrasound simulation (DELFI).
- Developed extensive experimental tools for imaging and data acquisition using the Sonix RP.
- Integrated a high frequency linear array probe with the Sonix RP to improve image and data quality.
- Built and expanded collaborations with numerous corporations including Philips Medical Systems, UltraSonix, InnerVision, and PocketSonics.
- Filed patent applications on FIR Beamforming, TONE, and qTONE.
- Licensed the FIR Beamforming algorithm to PocketSonics for use in its products.

Reportable Outcomes:

Papers:

1. Guenther, D.A., and W.F. Walker, "Broadband Optimal Contrast Resolution Beamforming," submitted to *IEEE Trans. Ultrason. Ferroelec. Freq. Contr.*, May 2007.
2. Guenther, D.A., Walker, W.F., "Optimal apodization design for medical ultrasound using constrained least squares, part I: theory," *IEEE Transactions on Ultrasonics, Ferroelectrics and Frequency Control*, vol. 54(2), pp. 332-342, 2007.
3. Viola, F., Ellis, M.A., Walker, W.F., "Time-domain optimized near-field estimator for ultrasound imaging: initial development and results," *IEEE Transactions on Medical Imaging*, vol. 27(1), pp. 99-110, 2008.
4. Ranganathan, K., Walker, W.F., "Cystic resolution: a performance metric for ultrasound imaging systems," *IEEE Transactions on Ultrasonics, Ferroelectrics and Frequency Control*, vol. 54(4), pp. 782-792, 2007.
5. Fuller, M.I., Blalock, T.N., Hossack, J.A., Walker, W.F., "Novel transmit protection scheme for ultrasound systems," *IEEE Transactions on Ultrasonics, Ferroelectrics and Frequency Control*, vol. 54(1), pp. 79-86, 2007.
6. Guenther, D.A., Walker, W.F., "Optimal apodization design for medical ultrasound using constrained least squares, part II: simulation results," *IEEE Transactions on Ultrasonics, Ferroelectrics and Frequency Control*, vol. 54(2), pp. 343-358, 2007.
7. Viola, F., Mauldin, F.W., Lin-Schmidt, X., Haverstick, D.M., Lawrence, M.B., Walker, W.F., "A novel ultrasound-based method to evaluate hemostatic function of whole blood," *Clinica Chimica Acta*, vol. 411(1-2), pp. 106-113, 2010.
8. Ellis, M.A., Guenther, D., Walker, W.F., "A spline-based approach for computing spatial impulse responses," *IEEE Transactions on Ultrasonics, Ferroelectrics and Frequency Control*, vol. 54(5), pp. 1045-1054, 2007.
9. Mauldin, F.W., Viola, F., Walker, W.F., "Reduction of echo decorrelation via complex principal component filtering," *Ultrasound in Medicine & Biology*, vol. 35(8), pp. 1325-1343, 2009.
10. Fuller, M.I., Ranganathan, K., Zhou, S., Blalock, T.N., Hossack, J.A., Walker, W.F., "Experimental system prototype of a portable, low-cost, c-scan, ultrasound imaging device," *IEEE Transactions on Biomedical Engineering*, vol. 55(2), pp. 519-530, 2008.
11. Guenther, D.A., Walker, W.F., "Receive channel FIR filters for enhanced contrast in medical ultrasound," *Medical Imaging 2007: Ultrasonic Imaging and Signal Processing Proceedings*, vol. 6513, San Diego, CA, Feb. 18, 2007.
12. Guenther, D.A., Walker, W.F., "A method for accurate in silico modeling of ultrasound transducer arrays," *Ultrasonics*, vol. 49(4-5), pp. 404-412, 2009.
13. Viola, F., Coe, R.L., Owen, K., Guenther, D.A., Walker, W.F., "Multi-dimensional spline-based estimator (MUSE) for motion estimation: algorithm development and initial results," *Annals of Biomedical Engineering*, vol. 36(12), pp. 1942-1960, 2008.
14. Guenther, D.A., Walker, W.F., "Generalized cystic resolution: a metric for assessing the fundamental limits on beamformer performance," *IEEE Transactions on Ultrasonics, Ferroelectrics and Frequency Control*, vol. 56(1), pp. 77-90, 2009.
15. Ellis, M.A., Viola, F., Walker, W.F., "Super-resolution image reconstruction using diffuse source models," *Ultrasound in Medicine & Biology*, vol. 36(6), pp. 967-977, 2010.

Conference Abstracts:

1. K. Owen and W.F. Walker, "A Novel Method for Designing and Fabricating Single Piston Transducers with Extended Depth of Field," submitted to the 2007 IEEE Ultrasonics Symposium.
2. M.A. Ellis, F. Viola, and W.F. Walker, "Diffuse Targets for Improved Contrast in Beamforming Adapted to Target," submitted to the 2007 IEEE Ultrasonics Symposium.
3. D.G. Guenther and W.F. Walker, "Optimal Contrast Resolution Beamforming," submitted to the

- 2007 IEEE Ultrasonics Symposium.
4. D.A. Guenther and W.F. Walker, "Receive Channel FIR Filters for Improved Contrast in Medical Ultrasound," 2007 SPIE Medical Imaging Symposium.
 5. F. Viola, M.A. Ellis, and W. F. Walker, "Near-Field, Broadband Adaptive Beamforming for Ultrasound Imaging," Fortieth Annual Asilomar Conference on Signals, Systems, and Computers, Pacific Grove, California, USA, 2006.
 6. M.A. Ellis and W.F. Walker, "Piecewise-Linear Approximation for Improved Accuracy in Near-Field Ultrasound Simulation," 2006 IEEE Ultrasonics Symposium.
 7. F. Viola, M.A. Ellis, and W.F. Walker, "Ultrasound Imaging with Beamforming Adapted to Target," 2006 IEEE Ultrasonics Symposium.
 8. D.A. Guenther, Ranganathan, K. and W.F. Walker, "Design of Apodization Profiles Using a Cystic Resolution Metric for Ultrasound," 2005 IEEE Ultrasonics Symposium.
 9. Viola, F. and W.F. Walker, "Adaptive Signal Processing in Medical Ultrasound Beamforming," 2005 IEEE Ultrasonics Symposium.
 10. Viola, F., and W.F. Walker, "Adaptive Beamforming for Medical Ultrasound Imaging," U.S. Dept. of Defense Breast Cancer Research Program Era of Hope 2005 Meeting, June 2005.

Patent Activity:

1. "Hybrid Dual Layer Diagnostic Ultrasound Transducer Array," J.A. Hossack, T.N. Blalock, W.F. Walker, U.S. Patent Application filed August 16, 2007.
2. "Intuitive Ultrasonic Imaging System and Related Method Thereof," W.F. Walker, J.A. Hossack, T.N. Blalock, U.S. Patent Application filed April 16, 2010.
3. "System and Method for Combined ECG-ECHO for Cardiac Diagnosis," A. Garson, W.F. Walker, J.A. Hossack, T.N. Blalock, U.S. Patent Application filed June 12, 2008.
4. "System and Method for Adaptive Beamforming for Image Reconstruction and/or Target/Source Localization," W.F. Walker and F. Viola, U.S. Patent Application filed September 19, 2006.
5. "An Improved Ultrasound Beamformer Using Channel Dependent FIR Filters," G.A. Guenther and W.F. Walker, provisional patent filed October 2, 2006.
6. "System and Method for Application of a Resolution Metric and Design for Apodization Profiles for Optimal Cystic Contrast," D.A. Guenther and W.F. Walker, patent disclosure filed September, 2005. (abandoned)
7. "Adaptive Beamforming for Medical Ultrasound Imaging," F. Viola, and W.F. Walker, patent disclosure filed 2005. (superceded by full application)

Software:

DELFI – A cubic spline based code for simulating spatial impulse responses. Available for download at:
<http://www.mathworks.com/matlabcentral/fileexchange/loadFile.do?objectId=13970>

Downloaded 227 times as of June 18, 2007.

Conclusions:

This research has shown the tremendous potential of novel image reconstruction methods. F IR Beamforming, which can be readily implemented in current imaging systems, yields substantial improvements in image contrast and resolution. The qTONE reconstruction algorithm yields dramatic improvements in image resolution and contrast. Further work will be needed to modify qTONE to reduce computational complexity to make it a viable real-time imaging tool. Initial work implementing the algorithm on graphics processors (GPUs) strongly suggest that real-time imaging with these methods will be feasible in a few years.

Bibliography:

1. Jackson, V.P., *The Role of US in Breast Imaging*. Radiology, 1990. **177**(2): p. 305 - 311.
2. Jackson, V., *Management of solid breast nodules: what is the role of sonography?* Radiology, 1995. **196**: p. 14-15.

3. Kolb, T.M., J. Lichy, and J.H. Newhouse, *Comparison of the Performance of Screening Mammography, Physical Examination, and Breast US and Evaluation of Factors that Influence Them: An Analysis of 27,825 Patient Evaluations*. Radiology, 2002. **225**: p. 165-175.
4. O'Donnell, M. and S.W. Flax, *Phase aberration correction using signals from point reflectors and diffuse scatters: measurements*. IEEE Trans. Ultrason. Ferroelec. Freq. Contr., 1988. **35**(6): p. 768-774.
5. O'Donnell, M. and S.W. Flax, *Phase aberration measurements in medical ultrasound: human studies*. Ultrasonic Imaging, 1988. **10**(1): p. 1-11.
6. Nock, L., G.E. Trahey, and S.W. Smith, *Phase aberration correction in medical ultrasound using speckle brightness as a quality factor*. JASA, 1989. **85**(5): p. 1819-1833.
7. Krishnan, S., P.-C. Li, and M. O'Donnell, *Adaptive Compensation of Phase and Magnitude Aberrations*. IEEE Transactions on Ultrasonics Ferroelectrics & Frequency Control, 1996. **43**(1): p. 44-55.
8. Hinkelman, L.M., D.L. Liu, and R.C. Waag, *Measurement and Correction of Ultrasonic Pulse Distortion Produced by the Human Breast*. Journal of the Acoustical Society of America, 1995. **97**(3): p. 1958-1969.
9. Ng, G.C., et al., *Speckle Target Adaptive Imaging Techniques for Distributed Phase Aberrations*. Ultrasonic Imaging, 1995. **17**(1): p. 63.
10. Zhu, Q. and B.D. Steinberg. *Correction of multipath interference using clean and spatial location diversity*. in *IEEE International Ultrasonics Symposium*. 1995. Seattle, Washington.
11. Rigby, K., et al. *Realtime Adaptive Imaging*. in *IEEE Ultrasonic Symposium*. 1998.
12. Rigby, K., et al. *Improved in vivo Abdominal Image Quality Using Real-Time Estimation and Correction of Wavefront Arrival Time Errors*. in *IEEE Ultrasonics Symposium*. 2000.
13. Gauss, R., G. Trahey, and M. Soo. *Wavefront Estimation in the Human Breast*. in *SPIE Medical Imaging*. 2001: SPIE.
14. Viola, F., Ellis, M.A., Walker, W.F., "Time-domain optimized near-field estimator for ultrasound imaging: initial development and results," *IEEE Transactions on Medical Imaging*, vol. 27(1), pp. 99-110, 2008.
15. Ranganathan, K., Walker, W.F., "Cystic resolution: a performance metric for ultrasound imaging systems," *IEEE Transactions on Ultrasonics, Ferroelectrics and Frequency Control*, vol. 54(4), pp. 782-792, 2007.
16. Guenther, D.A., Walker, W.F., "Generalized cystic resolution: a metric for assessing the fundamental limits on beamformer performance," *IEEE Transactions on Ultrasonics, Ferroelectrics and Frequency Control*, vol. 56(1), pp. 77-90, 2009.
17. Guenther, D.A., Walker, W.F., "Optimal apodization design for medical ultrasound using constrained least squares, part I: theory," *IEEE Transactions on Ultrasonics, Ferroelectrics and Frequency Control*, vol. 54(2), pp. 332-342, 2007.
18. Guenther, D.A., Walker, W.F., "Optimal apodization design for medical ultrasound using constrained least squares, part II: simulation results," *IEEE Transactions on Ultrasonics, Ferroelectrics and Frequency Control*, vol. 54(2), pp. 343-358, 2007.
19. Ellis, M.A., Guenther, D., Walker, W.F., "A spline-based approach for computing spatial impulse responses," *IEEE Transactions on Ultrasonics, Ferroelectrics and Frequency Control*, vol. 54(5), pp. 1045-1054, 2007.
20. Bethel, R., Shapo, B., Van Trees, H.L., "Single snapshot spatial processing: optimized and constrained," *Sensor Array and Multichannel Signal Processing Workshop Proceedings*, PP. 508-512, 2002.

Super-Resolution Image Reconstruction With Reduced Computational Complexity

Michael A. Ellis and William F. Walker, Ph.D.

Department of Biomedical Engineering
University of Virginia
UVa Health System
P.O. Box 800759
Charlottesville, VA 22908

Corresponding Author:
Name: Michael Ellis

Abstract:

We have previously described a new image reconstruction method called dTONE, which significantly increases both image contrast and resolution by conducting a global optimization based on a model of sparse hypothetical scatterer locations. Due to the large scale and $O(n^3)$ computational complexity, images of clinically significant dimensions would require approximately 33 days to reconstruct on a 3 GHz desktop computer. Here we describe an alternate algorithm - called quick-TONE, or qTONE - that provides a significant reduction in computational cost with improved image contrast under the conditions tested. Both methods, along with conventional image reconstruction, were applied to tissue mimicking phantoms and excised animal tissue. For the model used, qTONE provided an 8x reduction in computation time, a 2.7x reduction in memory requirements, and an 8 dB improvement in cystic contrast over the dTONE image.

INTRODUCTION

Unlike conventional image reconstruction (CIR) techniques in ultrasound, which throw away information in the received data when summing across channels, adaptive image reconstruction (AIR) methods make use of much of the information in the received data. Doing so allows AIR techniques to achieve resolutions beyond the diffraction limit along with improved image contrast. These enhancements could greatly improve the accuracy and precision of clinical diagnoses based on fine tissue structures such as small hepatic lesions [1], microcalcifications [2, 3], or spiculation [4]. However, the resolution and contrast improvements of AIR methods typically come at the cost of robustness to noise and aberration or greatly increased computational complexity.

One such AIR technique, called the Capon beamformer [5], has previously been applied to medical ultrasound with moderate success. As this method is sensitive to errors in the assumed wavefield parameters such as electronic noise and aberrations, techniques such as spatial smoothing [6, 7] and diagonal loading [8] must be used to increase the method's robustness. While these modifications do greatly increase the robustness of capon beamformers, they tend to significantly cannibalize the improved resolution and contrast such that there is little to no improvement over CIR methods [9]. In addition, capon beamformers for medical ultrasound require $O(n^3)$ calculations for each pixel in the reconstructed image, where n is the number of channels used to form the image. This computational burden makes real-time imaging unfeasible in the algorithm's current state.

We have previously described a new image reconstruction method called dTONE [10], which is well suited for ultrasound image reconstruction. Rather than estimate a set

of apodization weights for delay-and-sum imaging, this source localization technique uses an entirely different reconstruction framework to directly estimate the scatterer field, which allows it to achieve even greater resolution and contrast enhancement.

However, dTONE's resolution and contrast improvements come at the cost of a high computational burden. dTONE images of clinically significant dimensions would require 6.2 TB of memory and about 33 days of computation on a 3 GHz processor. CIR methods reconstruct images at upwards of 30 frames per second, visualizing human tissue in real-time and providing ultrasound with a major advantage over other medical imaging modalities, especially in cardiology applications. For these reasons, it is important that dTONE reconstructions be computed as close to real-time as possible. We have previously described a method to reduce computation times by parallelizing the algorithm using reduced rank sub-models [11]. Using this approach in simulation and experiment, image reconstruction time was decreased more than tenfold using 8 sub-models. A similar application of this approach to in vivo imaging would bring reconstruction time down from about 33 days to 3.3 days. Greater computational gains could be achieved using more sub-models at the expense of reconstruction image quality.

In order to further bring down the computational cost of dTONE such that it can be applied to in vivo imaging, a change in the core algorithm is required. Here we describe an alternative algorithm, called quick-TONE (qTONE), that is derived from the same foundation as dTONE. qTONE shifts the computational cost from being based on the number of hypothetical scatterers to being based on the number of input samples, which allows for significant reductions in reconstruction time with little effect on image quality. In this paper, the qTONE algorithm is derived and applied to tissue mimicking

phantoms and excised animal tissue to demonstrate its advantages over dTONE and CIR. Although qTONE is described here for typical transmit-receive ultrasound architecture, it also offers potential to significantly improve resolution and contrast in other image reconstruction architectures [12-14] and some novel passive ultrasound systems [15-17].

THEORY

From [18], the rate limiting step in the TONE algorithm is:

$$\underline{f}'_{free,k+1} = \left(\underline{P}_{free}^H \underline{T}_k \underline{P}_{fix} \right) \left(\underline{P}_{fix}^H \underline{T}_k \underline{P}_{fix} \right)^{-1} \underline{f}'_{fix} \quad (1)$$

The total computational cost of this calculation is approximately on the order of $fix^2(out + fix)$, where fix is the number of non-zero eigenvalues of $\underline{V}^H \underline{V}$ – which is at most equal to the number of channel-time samples – and out is the number of hypothetical scatterers in the output image. Here, fix is partly determined by the scale and spacing of the hypothetical scatterers in the ROI, binding the computational cost to the output sampling of dTONE. A decrease in the size of fix would substantially decrease the computational requirements of the reconstruction.

One simple way to achieve this goal is to adjust the cutoff between fix and $free$ – which sum together to equal the number of eigenvalues of $\underline{V}^H \underline{V}$ – such that some of the very small non-zero eigenvalues are treated as free parameters instead of fixed. As long as the non-zero eigenvalues that are rounded down to zero are small to begin with, there should be very little effect on reconstruction quality. This method, which is similar to principle component analysis, works well to reduce computational complexity but is limited in its efficacy due to a limited amount of flexibility before image degradation

becomes overly apparent. Empirical observations suggest the fix parameter can be reduced by no more than 10% before image degradation becomes noticeable. Considering a full breast image would require approximately 33 days to reconstruct on a 3 Ghz processor, far greater computational cost reductions are necessary to bring TONE to clinical feasibility.

QTONE DERIVATION

Ideally, the computational cost of the image reconstruction would be detached from the ROI spatial sampling so that large regions could be finely sampled without a significant increase in computational cost. To achieve this end, the TONE algorithm was reworked from its foundation. Recall from the derivation of TONE [19]:

$$\underline{x} = \underline{V}\underline{f} \quad (2)$$

where \underline{x} is the $NT \times 1$ data vector received by the N -element array, \underline{f} is the $LP \times 1$ target vector, whose elements are the amplitudes of the hypothetical targets located in the ROI, and \underline{V} is the $NT \times LP$ system model matrix. The maximum posterior estimate of \underline{f} is given by [20]:

$$\hat{\underline{f}} = \max_{\underline{f}} p(\underline{f} | \underline{x}) = \max_{\underline{f}} A p(\underline{x} | \underline{f}) p(\underline{f}) \quad (3)$$

where $p(\underline{x}, \underline{f})$ is the joint probability density function (PDF) and A is a normalizing constant that does not affect the maximum *a posteriori* estimate. We assume that the marginal PDF $p(\underline{f})$ is known *a priori* and mathematically expressed as a zero-mean Gaussian function [21, 22]:

$$p(\underline{f}) = \frac{1}{\pi^L \left| \underline{\underline{C}}_f \right|} \exp \left\{ -\underline{f}^H \underline{\underline{C}}_f^{-1} \underline{f} \right\} \quad (4)$$

Furthermore, $p(\underline{x}|\underline{f})$ is equally likely for every \underline{f} that satisfies the observation model in equation (2). Thus, equation (3) reduces to the following:

$$\hat{\underline{f}} = \max_{\underline{f}} p(\underline{f}) \quad (5)$$

which is referred to as the maximum *a posteriori* (MAP) estimate of \underline{f} .

Rather than maximize the actual PDF $p(\underline{f})$ as is done in TONE, we recognize that just maximizing the exponent should achieve the same purpose through a mathematically simpler means. Following on (4) and (5), after negating the exponent to form a cost minimization problem, we have:

$$\text{minimize } \underline{f}^H \underline{\underline{C}}_f^{-1} \underline{f} \quad \text{subject to} \quad \underline{x} = \underline{V} \underline{f} \quad (6)$$

This optimization problem is common in literature and using the Langrangian method [23], we solve for the MAP target vector as:

$$\hat{\underline{f}} = \underline{\underline{C}}_{\hat{\underline{f}}} \underline{V}^H \left(\underline{V} \underline{\underline{C}}_{\hat{\underline{f}}} \underline{V}^H \right)^{-1} \underline{x} \quad (7)$$

The introduction of a regularization term will aid in the inversion under certain difficult conditions where the reconstructed image is sparse:

$$\hat{\underline{f}} = \underline{\underline{C}}_{\hat{\underline{f}}} \underline{V}^H \left(\underline{V} \underline{\underline{C}}_{\hat{\underline{f}}} \underline{V}^H + \alpha \underline{I} \right)^{-1} \underline{x} \quad (8)$$

Starting with an initial guess, $\hat{\underline{f}}_0$, this can be solved non-linearly using the following

iteration:

$$\underline{\hat{f}}_{k+1} = \underline{C}_{\hat{f}_k} \underline{V}^H \left(\underline{V} \underline{C}_{\hat{f}_k} \underline{V}^H + \alpha \underline{I} \right)^{-1} \underline{x} \quad (9)$$

This process is stopped when the difference between successive estimates of \underline{f} drops below a desired threshold. The final $\underline{\hat{f}}_{k+1}$ is then reshaped and displayed on a log scale as the reconstructed image.

To further the robustness of the algorithm we include additive Gaussian noise in the linear model:

$$\underline{x} = \underline{V} \underline{f} + \underline{n} \quad (10)$$

where \underline{n} is the length LP noise vector. Applying this new model to (6) yields the solution for the MAP target vector:

$$\underline{\hat{f}}_{k+1} = \underline{C}_{\hat{f}_k} \underline{V}^H \left(\underline{V} \underline{C}_{\hat{f}_k} \underline{V}^H + \underline{C}_n \right)^{-1} \underline{x} \quad (11)$$

where \underline{C}_n is the noise covariance matrix. If we assume $\underline{C}_n = \alpha \underline{I}$, we arrive at the general Tikhonov regularized [24] form as given in (9). This Bayesian solution has been successfully applied in other fields such as magnetoencephalography [25], computed tomography [26], and positron emission tomography [27], but not medical ultrasound.

COMPUTATIONAL IMPLICATIONS

The total computational cost of this alternate calculation, called quick-TONE, or qTONE, is roughly on the order of $in^2(out + in)$, where in is the number of input sensor

array samples and *out* is the number of hypothetical scatterers in the output image; as opposed to the computational cost of standard dTONE, which is $fix^2(out + fix)$, where *fix* is the number of non-zero eigenvalues of $\underline{\underline{V}}^H \underline{\underline{V}}$. At first glance, qTONE does not provide a reduction in computational cost as *fix*, by definition, has a maximum value equal to *in*. However, the transfer of computational dependency from *fix* to *in* provides more freedom to intuitively reduce the computational complexity. Adjusting the balance between *fix* and *free* in dTONE provides a reduction in computational cost but quickly results in image degradation. In qTONE, an equivalent reduction in the number of input channel-time samples provides the same reduction in computational cost with far less image degradation.

Additionally, qTONE has far lower memory requirements than dTONE, significantly reducing the hardware requirements and further reducing reconstruction time due to reduced memory latencies. The memory requirements for dTONE are primarily determined by the total number of hypothetical sources used in the reconstruction. This is due to the need to store both the system model, $\underline{\underline{V}}$, and the eigen decomposition of $\underline{\underline{V}}^H \underline{\underline{V}}$. The matrix of eigenvectors is square with the dimensions of each side equal to the total number of hypothetical scatterers.

Images of clinically useful dimensions would require 1.2 TB to store the system model in memory and an additional 5.0 TB to store the matrix of eigenvectors. Assuming a very fast 408 GB/s memory bandwidth (NVIDIA® Tesla™ S1070), 12 seconds would be required just to access the matrix of eigenvectors as opposed to the 2.8 seconds required to access just the system model. As the computational cost is reduced

through the reduced rank tiling approach described in [28], this memory related latency becomes increasingly significant. Assuming 40 tiles and a system capable of 4 TFLOPS (NVIDIA® Tesla™ S1070), computation of dTONE without latencies would take about 5.5 seconds. Thus, an additional 6 second memory latency would more than double the computation time for image reconstruction. qTONE removes the requirement to store the matrix of eigenvectors and therefore significantly reduces reconstruction time by reducing memory latencies in addition to the direct computational cost reductions described above.

EFFICIENT COMPUTATION COST REDUCTION

qTONE's computational benefits come from a robustness to reductions in the number of input channel-time data. The simplest way to achieve this reduction is to directly downsample the channel-time data temporally. While this effectively decreases the reconstruction time, it does so at the expense of image quality as valuable information for the reconstruction is discarded. One equally simple, yet somewhat more robust method is to downsample the channel-time input data in a checker or pseudorandom pattern through both time and channel rather than just temporally. This method would maintain more temporal information at the expense of some channel information, which has been shown to not be a problem for tone reconstruction [18].

More elegant methods for reducing the size of the channel-time data exist that achieve similar computational improvements with even less image degradation. In order to reduce computational complexity while maintaining the most possible channel-time information, we first recognize that there is additional information in the sensor data that

is not necessary to form a high quality reconstructed image. By performing a singular value decomposition (SVD) on the manifold matrix, $\underline{\underline{V}}$, we can create a set of orthogonal vectors, $\underline{\underline{U}}$ and $\underline{\underline{W}}$, and their associated singular values, $\underline{\underline{S}}$.

$$\underline{\underline{V}} = \underline{\underline{U}} \underline{\underline{S}} \underline{\underline{W}}^H \quad (12)$$

Recalling the linear model from (2), we can substitute for $\underline{\underline{V}}$ to get:

$$\underline{\underline{x}} = \left(\underline{\underline{U}} \underline{\underline{S}} \underline{\underline{W}}^H \right) \underline{\underline{f}} \quad (13)$$

Multiplying both sides of the equation by $\underline{\underline{U}}^{-1}$ and rearranging terms yields:

$$\underline{\underline{x}}_p = \underline{\underline{V}}_p \underline{\underline{f}} \quad \text{where} \quad \underline{\underline{x}}_p = \underline{\underline{U}}^{-1} \underline{\underline{x}} \quad \text{and} \quad \underline{\underline{V}}_p = \left(\underline{\underline{S}} \underline{\underline{W}}^H \right) \quad (14)$$

So, by first performing an SVD on the system model, we can transform the sensor data and system model into a different space and then proceed as normal. By recognizing that not all the vectors and their associated singular values are necessary for accurate reconstruction, we can then reduce the dimensionality of the reconstruction. Thus, we threshold the singular values to a desired level – typically to maintain about 99% of the energy – and remove the associated basis vectors. The resulting reconstruction has reduced dimensionality but should still provide accurate image reconstruction as it maintains most of the important information and only eliminates the least important data.

ANECHOIC CYST PHANTOM

A 3 mm diameter, 7 cm long cylindrical anechoic cyst, surrounded by a 1 x 1 x 7 cm speckle-generating region was formed in 7% acrylamide gel. The 1 x 1 x 7 cm region of acrylamide gel containing SephadexTM G-50 Superfine scatterers (GE Healthcare) was

embedded in a larger block of acrylamide gel containing no scatterers such that the center of the cyst was at a depth of approximately 2 cm from the top of the phantom. An Ultrasonix Sonix RP system employing a 128 channel, 300 μm pitch, linear array was used to transmit a 6.6 MHz, 60% fractional bandwidth plane wave and obtain single channel RF data. The data was filtered using a 100-tap FIR filter with a pass-band from 3-10 MHz, demodulated to produce an IQ pair, and all but the center 64 channels were removed. The array manifold matrix was constructed by shifting and warping the spatial response from a single 20 μm diameter stainless steel wire embedded in the same 7% acrylamide gel at a depth of 2 cm. Elevation effects were not modeled for this set of experiments. Hypothetical targets were placed every 95.6 μm axially and every 120 μm laterally for both TONE and dTONE. The CIR image was formed using a 64 element, 300 μm pitch aperture on both transmit and receive, which is the standard configuration for the ultrasound system used. The transmit beam was focused at 2 cm and dynamic receive focusing was applied after band-pass filtering and apodization with a Nuttall window.

This system model has dimensions 13,632 x 18,471 samples with a total of 10,974 *fix* eigenvectors. Images were formed with progressively smaller rank in order to assess the computation time and reconstruction performance for dTONE as compared to qTONE using both simple temporal downsampling as well as SVD rank reduction. For qTONE, the input data was downsampled temporally by a factor of two and four so that only 6,848 and 3,424 input samples were included, respectively. QTONE was also rank reduced to those same levels using the SVD method described above. Likewise, for dTONE, the balance between *fix* and *free* was adjusted so that only 6,848 and 3,424

eigenvectors were included in the *fix* set. In this way, the computation time and reconstruction performance of dTONE was compared with those of the two qTONE methods for three different levels of rank reduction.

The results from these experiments are shown in Figure 1 through Figure 3 and Table 1. qTONE using both temporal downsampling and SVD rank reduction achieves improved image quality and reduced computation time compared to dTONE in the reduced rank examples. Both of the qTONE methods achieve an additional computation cost reduction – as much as 44% – due to the reduced memory access requirements. qTONE at rank 6,848 achieves an 8.4 dB contrast improvement over full rank dTONE while also reducing the computation time by a factor of 8.

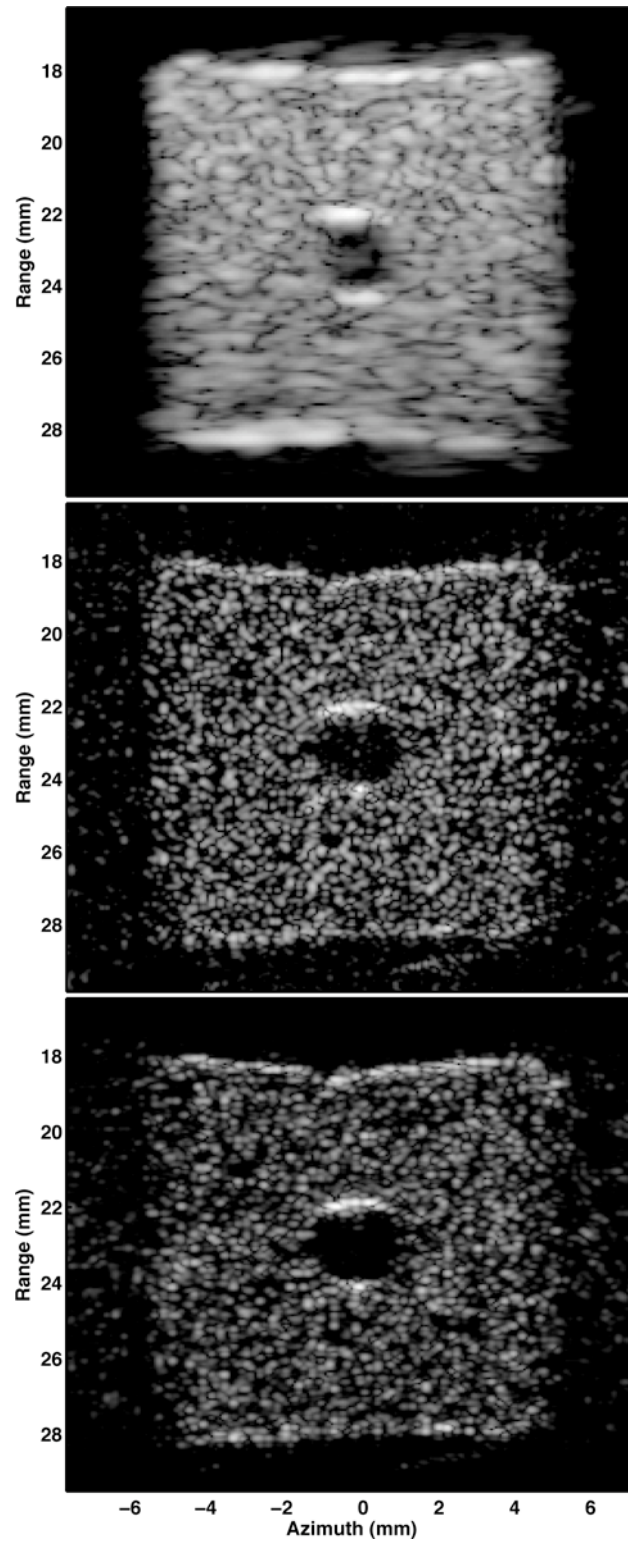


Figure 1. Experimental images of an anechoic cyst phantom comparing full rank reconstruction performance of CIR (top), rank 10,974 dTONE (middle), and rank 13,696 qTONE (bottom). All images are log compressed to 50 dB.

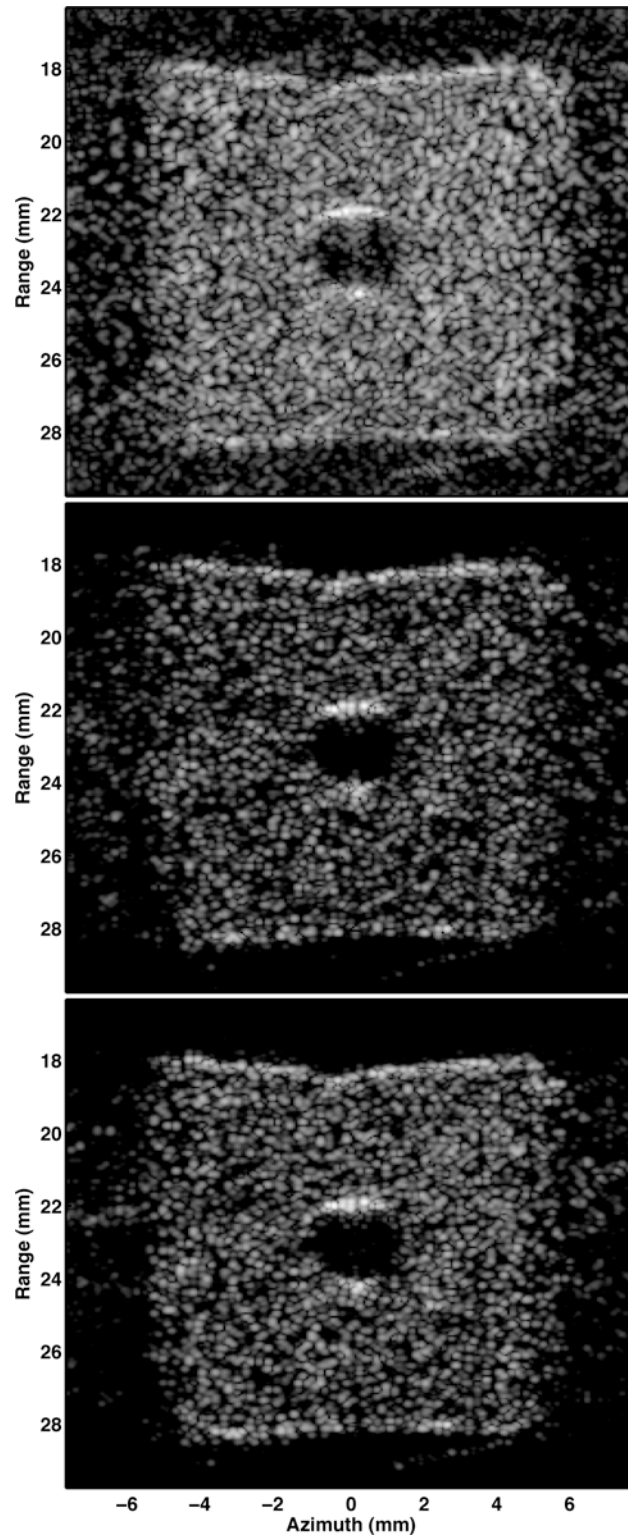


Figure 2. Experimental images of an anechoic cyst phantom comparing reduced rank (rank 6848) reconstruction performance of dTONE (top), temporally downsampled qTONE (middle), and SVD downsampled qTONE (bottom). All images are log compressed to 50 dB.

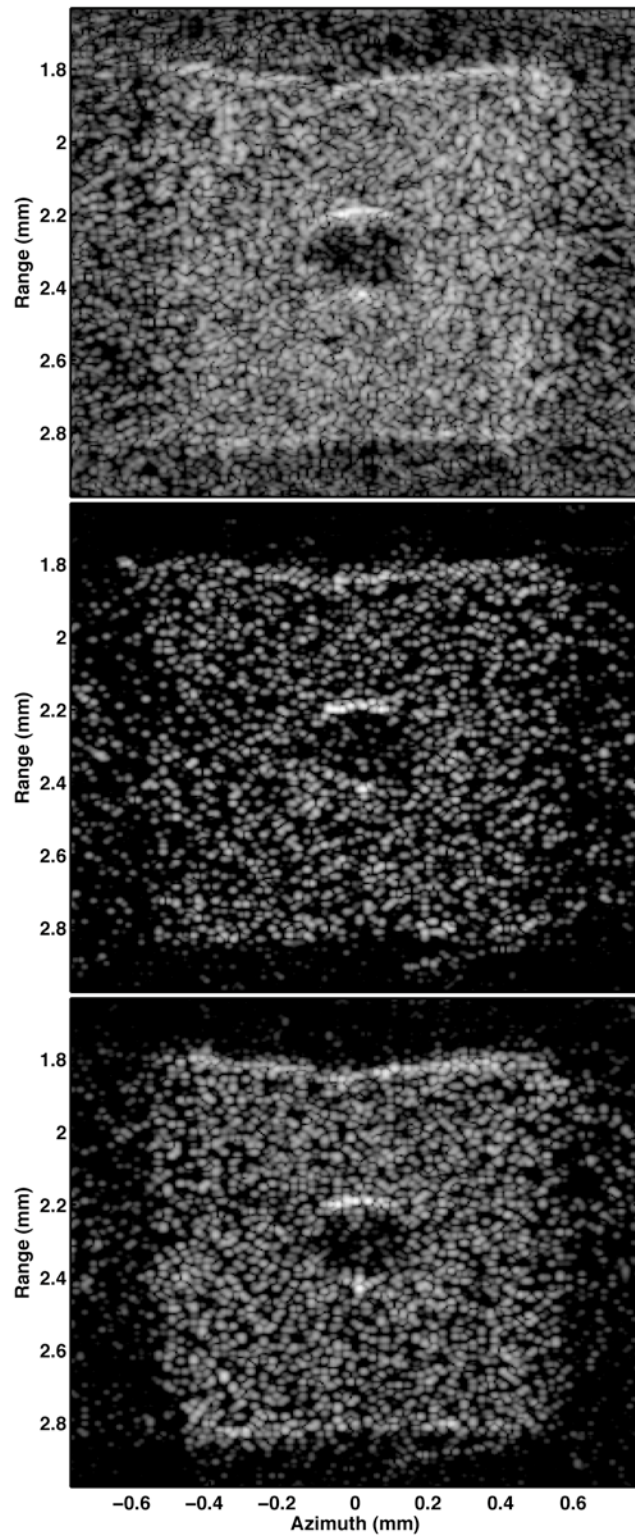


Figure 3. Experimental images of an anechoic cyst phantom comparing reduced rank (rank 3424) reconstruction performance of dTONE (top), temporally downsampled

qTONE (middle), and SVD downsampled qTONE (bottom). All images are log compressed to 50 dB.

TABLE 1. EXPERIMENTAL COMPARISON OF REDUCED RANK IMAGE RECONSTRUCTION METHODS.

Reconstruction Method	Total Memory (GB)	Computation Time (min)	Cystic Contrast (dB)
CIR	-	-	-6.4
Rank 10,974/13,632			
dTONE	9.5	64.6	-14.4
qTONE	4.0	61.3	-14.9
Rank 6,848			
dTONE	9.5	14.3	-11.7
qTONE (temporal)	2.0	8.0	-22.2
qTONE (SVD)	3.5	8.1	-22.8
Rank 3,424			
dTONE	9.5	4.4	-10.8
qTONE (temporal)	1.0	2.8	-10.4
qTONE (SVD)	1.8	2.9	-11.9

ANIMAL TISSUE PHANTOMS

An excised mouse heart was flushed with phosphate-buffered solution (PBS) to remove any remaining blood from the chambers and then embedded at a depth of 2 cm in a block of 7% acrylamide gel. Effort was taken to ensure the chambers of the heart remained in an open state by backfilling them with 7% acrylamide prior to embedding the heart. Additionally, a 3 cm length of aorta was excised from a rabbit, flushed with PBS, and backfilled with 7% acrylamide prior to embedding it in a block of 7% acrylamide at a depth of 2 cm. Both tissue samples were then imaged using the same parameters used for the anechoic cyst phantom, with dTONE operating at full rank (rank 10,974) and qTONE at rank 6,848. Again, elevation slice thickness was not modeled.

Results from the tissue phantoms are shown in Figure 4. True quantitative

measurements couldn't be made in the animal tissue experiments due to an unknown ground truth. Although both dTONE images demonstrate enhanced contrast and resolution, delineation of tissue boundaries is still somewhat difficult, especially in the mouse heart image. The qTONE images, however, show a superior delineation of the boundary between the septum and the anechoic ventricles due to increased contrast when compared to dTONE. In addition, the increased contrast of qTONE comes paired with an 8x reduction in computation time and a 2.7x reduction in memory requirements.

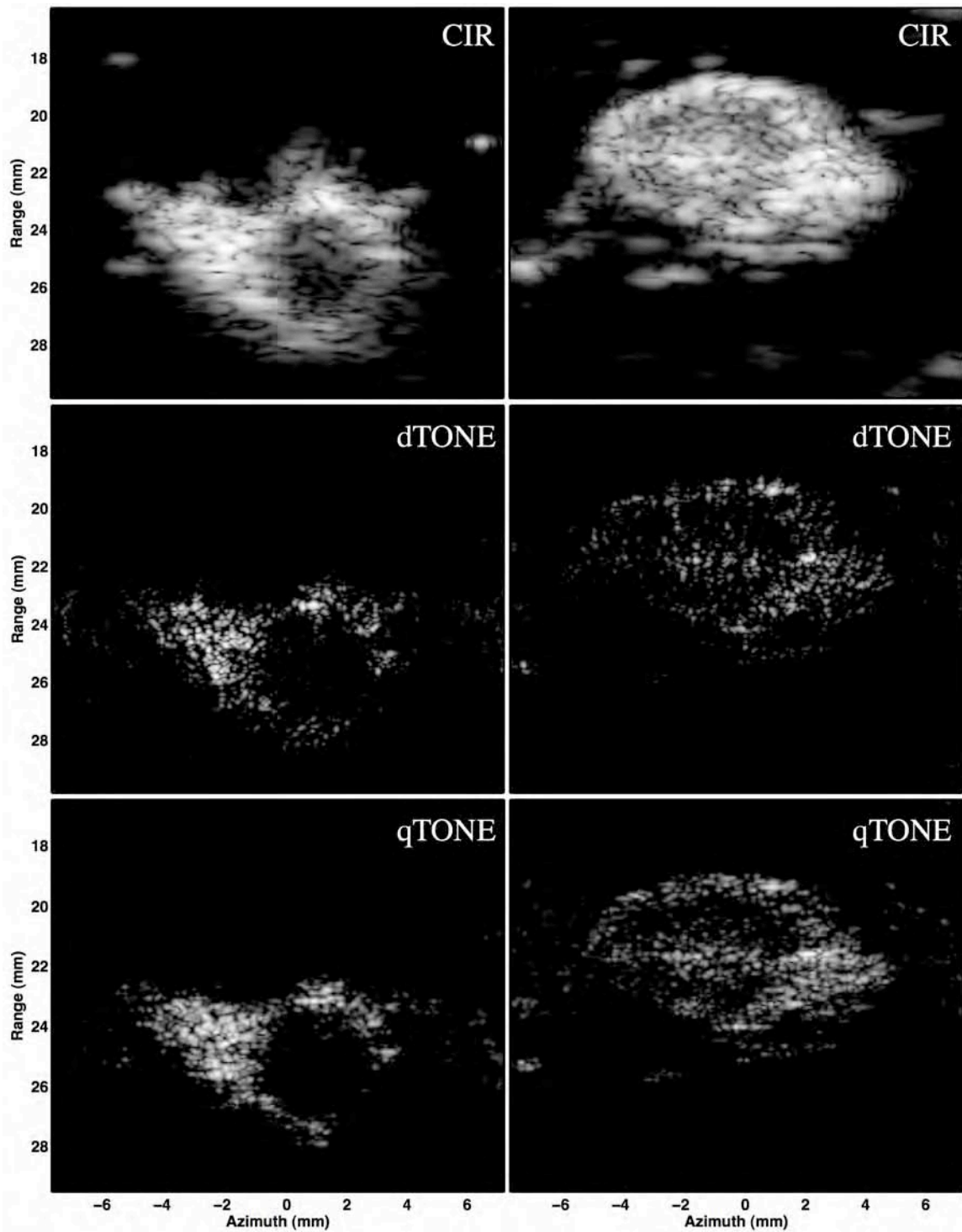


Figure 4. Experimental excised animal tissue reconstructions using CIR (top row), full-rank dTONE (middle row), and rank 6848 qTONE (bottom row). The left column contains reconstructions of an excised section of rabbit aorta and the right column contains a long-axis view of an excised mouse heart. Both tissues are embedded in acrylamide gel. All images are log compressed to 50 dB.

DISCUSSION

Images reconstructed using the dTONE algorithm display significantly improved resolution and contrast when compared to those from CIR. The enhanced image quality could lead to improvements in diagnosis sensitivity and specificity, but those gains come with a significant increase in the computation required to reconstruct images. For dTONE to be considered as a viable alternative or auxiliary to CIR, the reconstruction times must be reduced to near real-time for images of clinically significant dimensions. The qTONE algorithm presented here successfully reduced the computational cost by a factor of eight while simultaneously improving the measured cystic contrast and by a factor of twenty with a small loss in image quality. By combining the two approaches, tiled qTONE could achieve reductions in computation cost of more than 4 orders of magnitude with only a small loss in image quality.

The inclusion of noise in the system model, as in (10), is important for the practical application of qTONE in clinical environments. The amount of regularization necessary depends heavily upon the amount of noise present in the data, which varies depending upon the type of tissue being imaged and at what depth. Assuming a fixed amount of attenuation in specific tissues, we can vary the regularization for tiled qTONE as the tiles progress in depth. Doing so will ensure that each tile is optimally reconstructed. In a practical implementation, it may also be beneficial to have a user controllable dial that would increase or decrease the regularization a small percent from the automatically chosen value.

Although [10] demonstrates dTONE's robustness to electronic noise and phase and magnitude aberration, it does not necessarily follow that qTONE has similar

robustness characteristics. To fully explore these traits, a similar set of simulations should be performed comparing qTONE to both dTONE and CIR. Although electronic noise robustness simulations would also be important, the 40 dB SNR explored in this paper might prove sufficient given dTONE's single transmit event requirement, which enables averaging over 100 separate transmits in less than 0.01 seconds. In addition, other methods such as coded excitation could be used to ensure high SNR levels, even at greater depths where attenuation significantly reduces SNR. A lower transmit pulse center frequency would also increase the SNR at the expense of some spatial resolution and be less susceptible to phase aberration errors.

CONCLUSIONS

In this paper, an alternative to the dTONE image reconstruction algorithm – derived from the same foundations – is derived and evaluated. This algorithm, called Quick TONE, or qTONE, is far more robust than dTONE to reductions in system model rank. As a result, qTONE can reconstruct images of equal or greater contrast with far less computational and memory requirements. In addition, a sophisticated approach to reducing the qTONE model rank is presented that further improves the algorithm's robustness to rank reduction. For the system models tested here, qTONE showed an 8x decrease in computation time, but this difference should increase as the size of the model increases, bringing clinical super-resolution images closer to reality.

- [1] S. Eberhardt, P. Choi, A. Bach, S. Funt, H. Felderman, and L. Hann, "Utility of sonography for small hepatic lesions found on computed tomography in patients with cancer," *Journal of Ultrasound in Medicine*, vol. 22, pp. 335, 2003.
- [2] M. E. Anderson, M. S. Soo, R. C. Bentley, and G. E. Trahey, "The detection of breast microcalcifications with medical ultrasound," *Journal of the Acoustical Society of America*, vol. 101, pp. 29-39, 1997.
- [3] W. T. Yang, M. Suen, A. Ahuja, and C. Metreweli, "In vivo demonstration of microcalcification in breast cancer using high resolution ultrasound," *The British Journal of Radiology*, vol. 70, pp. 685-690, 1997.
- [4] S.-F. Huang, R.-F. Chang, D.-R. Chen, and W. K. Moon, "Characterization of spiculation on ultrasound lesions," *Medical Imaging, IEEE Transactions on*, vol. 23, pp. 111-121, 2004.
- [5] J. Capon, "High-resolution frequency-wavenumber spectrum analysis," *Proceedings of the IEEE*, vol. 57, pp. 1408-1418, 1969.
- [6] J.-F. Synnevag, A. Austeng, and S. Holm, "Adaptive Beamforming Applied to Medical Ultrasound Imaging," *Ultrasonics, Ferroelectrics and Frequency Control, IEEE Transactions on*, vol. 54, pp. 1606-1613, 2007.
- [7] M. Sasso and C. Cohen-Bacrie, "Medical ultrasound imaging using the fully adaptive beamformer," *Acoustics, Speech, and Signal Processing, 2005. Proceedings.(ICASSP'05). IEEE International Conference on*, vol. 2, 2005.
- [8] F. Vignon and M. R. Burcher, "Capon beamforming in medical ultrasound imaging with focused beams," *Ultrasonics, Ferroelectrics and Frequency Control, IEEE Transactions on*, vol. 55, pp. 619-628, 2008.
- [9] A. Austeng, T. Bjastad, J.-F. Synnevaag, S.-E. Masoy, H. Torp, and S. Holm, "Sensitivity of minimum variance beamforming to tissue aberrations," presented at Ultrasonics Symposium, 2008. IUS 2008. IEEE Ultrasonics Symposium, 2008. IUS 2008. IEEE VO -, 2008.
- [10] M. A. Ellis, F. Viola, and W. F. Walker, "Super-Resolution Image Reconstruction Using Diffuse Target Models," *Ultrasound in Medicine & Biology*, Submitted for review.
- [11] M. A. Ellis and W. F. Walker, "Reduced rank formulation for increased computational efficiency in medical ultrasound model-based beamforming," presented at 42nd Asilomar Conference on Signals, Systems and Computers, 2008.
- [12] M. Fink, L. Sandrin, M. Tanter, S. Catheline, S. Chaffai, J. Bercoff, and J. Gennisson, "Ultra high speed imaging of elasticity," presented at 2002 IEEE Ultrasonics Symposium, 2002. Proceedings, 2002.
- [13] M. I. Fuller, E. V. Brush, M. D. C. Eames, T. N. Blalock, J. A. Hossack, and W. F. Walker, "The Sonic Window: Second Generation Prototype of a Low-Cost, Fully Integrated, Pocket-Sized Medical Ultrasound Device," presented at IEEE Ultrasonics Symposium, Montreal, Canada, 2005.
- [14] M. Tanter, J. Bercoff, L. Sandrin, and M. Fink, "Ultrafast compound imaging for 2-D motion vector estimation: application to transient elastography," *IEEE Transactions on Ultrasonics Ferroelectrics & Frequency Control*, vol. 49, pp. 1363-74, 2002.
- [15] S. Sethuraman, S. Aglyamov, J. Amirian, R. Smalling, and S. Emelianov,

- "Intravascular photoacoustic imaging using an IVUS imaging catheter," *IEEE Transactions on Ultrasonics, Ferroelectrics and Frequency Control*, vol. 54, pp. 978-986, 2007.
- [16] V. Kozhushko, T. Khokhlova, A. Zharinov, I. Pelivanov, V. Solomatin, and A. Karabutov, "Focused array transducer for two-dimensional photoacoustic tomography," *The Journal of the Acoustical Society of America*, vol. 116, pp. 1498, 2004.
- [17] S. Emelianov, S. Aglyamov, J. Shah, S. Sethuraman, W. Scott, R. Schmitt, M. Motamedi, A. Karpouk, and A. Oraevsky, "Combined ultrasound, photoacoustic and elasticity imaging," presented at Proceedings of the 2004 SPIE Photonics West Symposium: Photons Plus Ultrasound: Imaging and Sensing, 2004.
- [18] F. Viola, M. A. Ellis, and W. F. Walker, "Time-Domain Optimized Near-Field Estimator for Ultrasound Imaging: Initial Development and Results," *Medical Imaging, IEEE Transactions on*, vol. 27, pp. 99-110, 2008.
- [19] F. Viola, M. Ellis, and W. Walker, "Ultrasound Imaging with Beamforming Adapted to Target," *Ultrasonics Symposium, 2006. IEEE*, pp. 128-131, 2006.
- [20] L. L. Scharf, *Statistical Signal Processing: Detection, Estimation and Time Series Analysis*. Reading, MA: Addison-Wesley Publishing Company, 1990.
- [21] R. F. Wagner, S. W. Smith, J. M. Sandrik, and H. Lopez, "Statistics of speckle in ultrasound B-scans," *IEEE Transactions on Sonics and Ultrasonics*, vol. 30, pp. 156-163, 1983.
- [22] E. Levitan and G. T. Herman, "A Maximum a Posteriori Probability Expectation Maximization Algorithm for Image Reconstruction in Emission Tomography," *Medical Imaging, IEEE Transactions on*, vol. 6, pp. 185-192, 1987.
- [23] A. P. Schachat, R. P. Murphy, and A. Patz, *Medical Retina*, vol. 2, 1 ed. St. Louis: The C. V. Mosby Company, 1989.
- [24] C. R. Vogel, *Computational Methods for Inverse Problems*. Philadelphia: SIAM, 2002.
- [25] J. W. Phillips, R. M. Leahy, and J. C. Mosher, "MEG-based imaging of focal neuronal current sources," presented at Nuclear Science Symposium and Medical Imaging Conference Record, 1995., 1995 IEEE, 1995.
- [26] K. M. Hanson and G. W. Wecksung, "Bayesian approach to limited-angle reconstruction in computed tomography," *J. Opt. Soc. Am. Journal of the Optical Society of America*, vol. 73, pp. 1501-1509, 1983.
- [27] C.-T. Chen, V. E. Johnson, W. H. Wong, X. Hu, and C. E. Metz, "Bayesian image reconstruction in positron emission tomography," *Nuclear Science, IEEE Transactions on*, vol. 37, pp. 636-641, 1990.
- [28] M. Ellis, F. Viola, and W. Walker, "Diffuse Targets for Improved Contrast in Beamforming Adapted to Target," *IEEE Ultrasonics Symposium*, pp. 216-219, 2007.

Abstract:

We have previously introduced a new image reconstruction method that significantly increases both image contrast and resolution and described important modifications to this algorithm that increase its robustness to variations from the model and significantly reduce computation costs. The modified versions of this algorithm, called TONE, were validated and compared to CIR techniques through application to simulated data as well as tissue mimicking phantoms and excised animal tissue. However, these simulations and experiments were conducted under a limited set of conditions that don't necessarily translate well to clinical imaging environments. Here we reconstruct the first set of *in vivo* images using all of the techniques introduced in this dissertation and qualitatively compare the results to CIR. In the two different *in vivo* views of a human testicle shown, the modified TONE reconstruction demonstrates significant improvement in image quality over that of CIR.

INTRODUCTION

TONE is a new image reconstruction method for medical ultrasound that is based on a source localization technique using a well-defined system model. In its original form, TONE showed significant promise for increasing resolution and contrast of ultrasound images, but was not well suited for clinical imaging due to limited robustness to model variations and significant computational costs. We have previously described a modification to the TONE algorithm that improves robustness of the reconstruction by modeling hypothetical scatterers as weighted, diffuse regions of scatterers [1]. The modification, called diffuse-TONE, or dTONE, proved robust to electronic noise and aberration in simulated datasets. In addition, the modified algorithm was applied to tissue mimicking phantoms and excised animal tissue with success. We have also previously described a method to achieve much of the computational gains from parallelization with little of the loss in reconstruction fidelity [2]. The approach uses rank reduction to efficiently model all potential sources outside the borders of each sub-model. In both simulation and experiment with tissue mimicking phantoms, this technique demonstrated a greater than ten-fold reduction in computation cost with only a small loss in image quality. We have also described an alternative algorithm to TONE, called quick-TONE, or qTONE, that is derived from the same foundations and produces nearly equivalent or better results with further reduced computation time.

With the significant computational gains of tiled qTONE and the robustness improvements of dTONE, *in vivo* imaging is now possible on readily available hardware. In this paper we describe an experiment imaging a human testicle *in vivo*. Reconstructed images from tiled qTONE are shown to display significant improvements in image

quality and feature detectability as compared to CIR methods.

6.2 EXPERIMENTAL METHODS AND RESULTS

An Ultrasonix Sonix RP system employing a 128 channel, 300 μm pitch, linear array was used to image a human testicle *in vivo*. A 6.6 MHz, 60% -6dB fractional bandwidth plane wave was used on transmit and single channel RF data was received. The received data was filtered using a 100-tap FIR filter with a pass-band from 3-10 MHz, demodulated to produce an IQ pair, and all but the center 64 channels were removed. The CIR image was formed using a 64 element, 300 μm pitch aperture on both transmit and receive, which is the standard configuration for the ultrasound system used. The transmit beam was focused at 2 cm and dynamic receive focusing was applied after band-pass filtering and apodization with a Nuttall window.

The array manifold matrix was constructed by shifting and warping the spatial response from a single 20 μm diameter stainless steel wire embedded in 7% acrylamide gel at a depth of 2 cm. Elevation effects were not modeled for this set of experiments. Hypothetical scatterers were placed every 95.6 μm axially and every 120 μm laterally over a 4 cm by 5 cm region, for a total of 173,888 hypothetical scatterers. Although the model covered a 5 cm region in azimuth, only the middle 3 cm were fully reconstructed so as to match the dimensions of the CIR image. As such, the outer 1 cm on each side in azimuth were rank reduced to about 1/3 the size using principal component analysis, as described in [2]. The model used for these experiments thus contains 104,500 full hypothetical scatterers and about 22,900 reduced rank hypothetical scatterers. Along with the 47,000 IQ samples for each hypothetical scatterer, the total memory required for such a model is 96 GB. The fully modeled 4 cm by 3 cm region was then sub-divided

into 8 tiles with 50% overlap using the temporal tiling method described in [2] and then processed using qTONE. The model for each tile, therefore, contained 32,162 fully modeled scatterers and 31,800 reduced rank hypothetical scatterers and required 10.7 GB of memory. The total reconstruction time for all tiles computed in parallel was 18.5 minutes.

The Sonix RP system used for this study does not have the capability to receive and store 64 raw RF lines in parallel. As a result, 64 separate plane wave transmit events were required to obtain the necessary data for tiled qTONE. This additional time requirement for data acquisition has the potential to introduce motion artifacts, which could severely diminish qTONE reconstruction quality. To compensate, a tracking beam was interspersed at a constant interval – every fifth transmit event for the experiments in this paper – among the plane wave transmit, single channel receive events. This tracking beam consists of a transmit focused down the center of the array at a depth of 2 cm with dynamic receive focusing. At the end of data acquisition, the tracking beams were parsed from the single channel data and the beam-to-beam displacements were determined using cubic spline based time delay estimation [3]. The required motion correction for each single channel data line was then calculated using cubic interpolation between the displacements of the surrounding tracking beams. Finally, the motion correction was applied using cubic spline interpolation to shift the RF data lines.

The reconstructed images from two different views of the testicle are shown in Figure 1 and Figure 2. As the ground truth anatomy for these views is unknown, only qualitative analysis can be conducted. However, in both image views, the tiled qTONE image demonstrates significantly improved delineation of tissue boundaries and clutter

reduction. In Figure 1, there are two distinct oval shaped anechoic regions at a depth of about 17 mm. The leftmost of these two regions is barely detectable in the CIR image but is clearly delineated in the tiled qTONE image. The enhanced contrast and resolution of the tiled qTONE reconstruction also shows a significant increase in apparent size of the rightmost of these two regions. Very similar results are seen in the anatomical view of Figure 2; especially with the three anechoic vessels between 19 mm and 23 mm in range, which are clearly detected in the tiled qTONE reconstruction but barely visible in the CIR image.

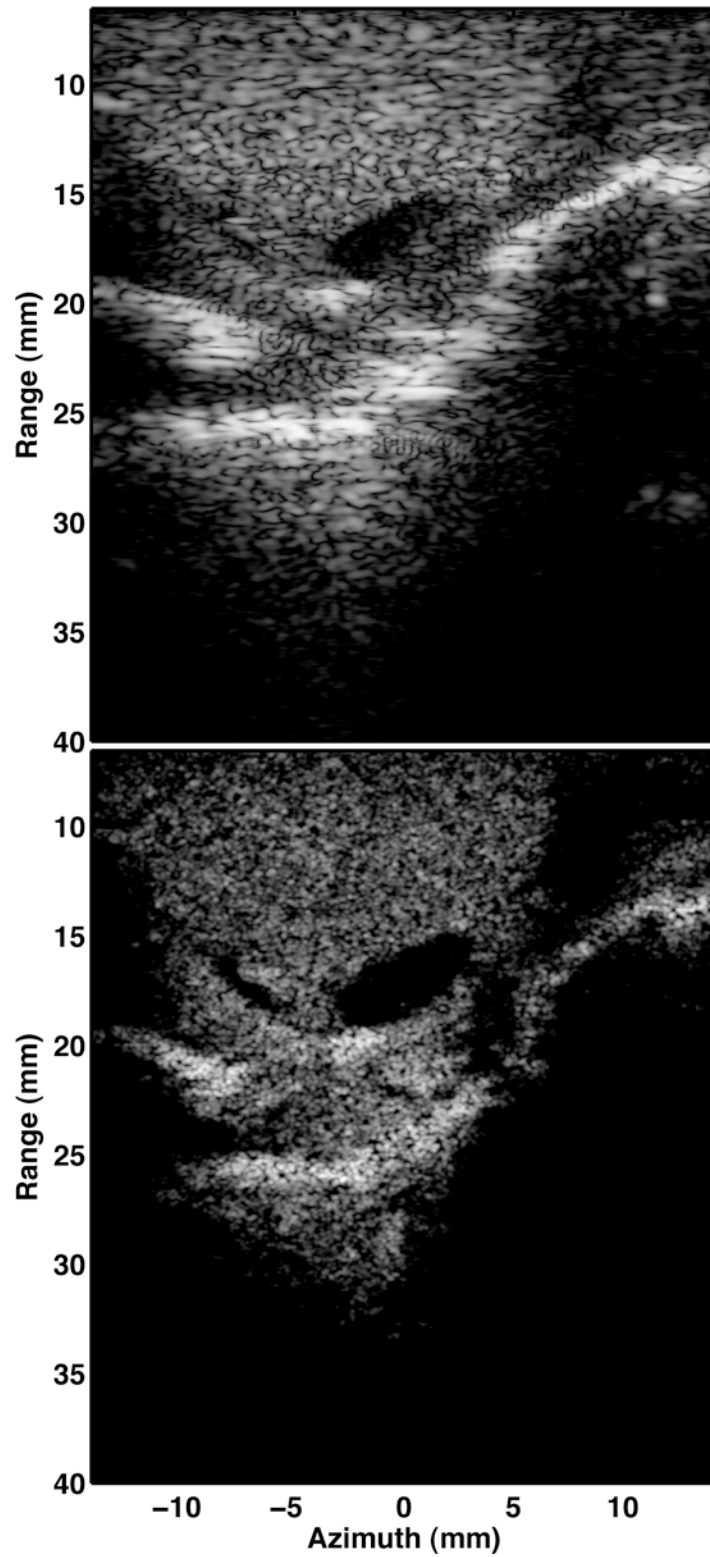


Figure 1. *In vivo* CIR (top) and tiled qTONE (bottom) images of a human testicle. All images log compressed to 50 dB.

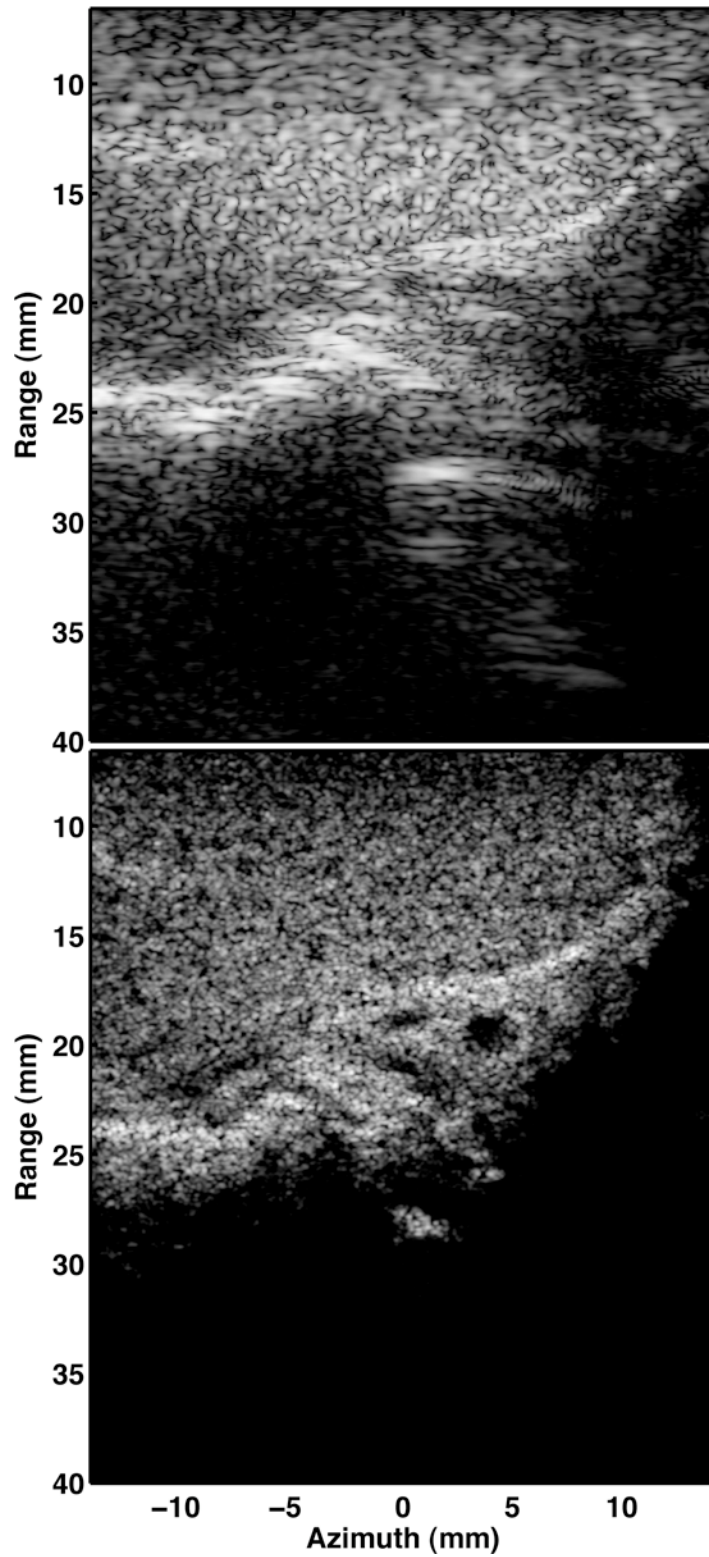


Figure 2. *In vivo* CIR (top) and tiled qTONE (bottom) images of a human testicle. All images log compressed to 50 dB.

DISCUSSION

The results shown in this paper are the first demonstration of a source localization technique applied to in vivo ultrasound data. Although the anatomy of the imaged tissue – a human testicle – isn't overly complex, there are enough tissue boundaries and features to highlight tiled qTONE's benefits over CIR methods. The significant increase in resolution and contrast of tiled qTONE bring out otherwise undetectable features in the anatomy shown in these images. Additionally, tiled qTONE shows enhanced tissue boundary delineation for those features that are detected in the CIR images. Such improvements could have significant implications for the diagnostic capabilities of medical ultrasound. The ability to reliably resolve features such as spiculation [4] or microcalcifications [5-7] in breast imaging, for example, could lead to earlier and more accurate diagnoses and may even cause ultrasound to supplant mammography in certain applications.

The system model matrix used in these experiments was not formed in an ideal manner for optimal reconstruction performance. The system response of each hypothetical scatterer was determined by shifting and warping the measured response from a 20 μm diameter stainless steel wire embedded in 7% acrylamide gel, making it a hybrid of an experimental and a theoretical model. This process of shifting and warping a single measured response is prone to introducing artifacts in the reconstructed image, as it does not take into account factors such as element directivity and frequency dependent attenuation. Ideally the system model matrix would be determined entirely through experiment, mimicking in vivo acoustic parameters as closely as possible. Using such a system model should be expected to result in higher quality reconstructions with reduced

image artifact.

The tiled qTONE image reconstructions in this paper took approximately 18.5 minutes to compute in parallel on eight 2.33 GHz processors. While this amount of time is reasonable for laboratory experiments, it would not suffice for clinical imaging environments, where real-time reconstruction is essential. Nevertheless, there are several possibilities for further reducing computation time to achieve real-time reconstruction. Thanks to continuing computational advances, there currently exist off-the-shelf systems capable of 4 TFLOPS, with more than 400 GB/s memory bandwidth (Nvidia® Tesla™ S2070). Using such a system would bring the reconstruction time for the images shown in this paper down from 18.5 minutes to 0.5 seconds. Although that is still about an order of magnitude short of real-time image reconstruction, there is potential to reduce computation time further by breaking the reconstruction up into more tiles.

CONCLUSIONS

In this paper, all of the previously described TONE methods were applied to *in vivo* data from a human testicle. The result is the first application of a source localization technique to *in vivo* ultrasound data. The tiled qTONE images show a marked improvement in tissue boundary delineation and contrast when compared to their CIR counterparts. Although the tiled qTONE images in this paper required 18.5 minutes to reconstruct, off-the-shelf hardware is available that would bring the computation time down to 0.5 seconds. Further reconstruction time reductions could also be achieved by increasing the number of tiles used, bringing real-time super-resolution imaging closer to reality.

- [1] M. A. Ellis, F. Viola, and W. F. Walker, "Super-Resolution Image Reconstruction Using Diffuse Target Models," *Ultrasound in Medicine & Biology*, Submitted for review.
- [2] M. A. Ellis and W. F. Walker, "Reduced rank formulation for increased computational efficiency in medical ultrasound model-based beamforming," presented at 42nd Asilomar Conference on Signals, Systems and Computers, 2008.
- [3] F. Viola and W. F. Walker, "A Spline Based Algorithm for Continuous Time Delay Estimation Using Sampled Data," *IEEE Transactions on Ultrasonics Ferroelectrics & Frequency Control*, vol. 52, pp. 80-93, 2005.
- [4] S.-F. Huang, R.-F. Chang, D.-R. Chen, and W. K. Moon, "Characterization of spiculation on ultrasound lesions," *Medical Imaging, IEEE Transactions on*, vol. 23, pp. 111-121, 2004.
- [5] M. E. Anderson, M. S. Soo, R. C. Bentley, and G. E. Trahey, "The detection of breast microcalcifications with medical ultrasound," *Journal of the Acoustical Society of America*, vol. 101, pp. 29-39, 1997.
- [6] J. R. Cleverley, A. R. Jackson, and A. C. Bateman, "Pre-operative localization of breast microcalcifications using high-frequency ultrasound," *Clinical Radiology*, vol. 52, pp. 924-926, 1997.
- [7] W. T. Yang, M. Suen, A. Ahuja, and C. Metreweli, "In vivo demonstration of microcalcification in breast cancer using high resolution ultrasound," *The British Journal of Radiology*, vol. 70, pp. 685-690, 1997.